APS physics

CHORUS

This is the accepted manuscript made available via CHORUS. The article has been published as:

Comparison of the lattice Boltzmann equation and discrete unified gas-kinetic scheme methods for direct numerical simulation of decaying turbulent flows

Peng Wang, Lian-Ping Wang, and Zhaoli Guo

Phys. Rev. E **94**, 043304 — Published 13 October 2016

DOI: 10.1103/PhysRevE.94.043304

Comparison of the LBE and DUGKS methods for DNS of decaying turbulent flows

Peng Wang,[1] Lian-Ping Wang,[1,2] and Zhaoli Guo[1,*]

[1]*State Key Laboratory of Coal Combustion,*
Huazhong University of Science and Technology, Wuhan 430074, China

[2]*Department of Mechanical Engineering,*
University of Delaware, Newark, DE 19716, USA

(Dated: September 23, 2016)

Abstract

The main objective of this work is to perform a detailed comparison of the lattice Boltzmann equation (LBE) and the recently developed discrete unified gas-kinetic scheme (DUGKS) methods for direct numerical simulation (DNS) of the decaying homogeneous isotropic turbulence (DHIT) and the Kida vortex flow in a periodic box . The flow fields and key statistical quantities computed by both methods are compared with those from pseudo-spectral (PS) method at both low and moderate Reynolds numbers. The results show that the LBE is more accurate and efficient than the DUGKS, but the latter has a superior numerical stability, particularly for high Reynolds number flows. In addition, we conclude that the DUGKS can adequately resolve the flow when the minimum spatial resolution parameter $k_{max}\eta > 3$, where k_{max} is the maximum resolved wavenumber and η is the flow Kolmogorov length. This resolution requirement can be contrasted to the requirements of $k_{max}\eta > 1$ for the pseudo-spectral method and $k_{max}\eta > 2$ for LBE. It should be emphasized that although more validations should be conducted before the DUGKS can be called a viable tool for DNS of turbulent flows, the present work contributes to the overall assessment of the DUGKS, and provides a basis for further applications of DUGKS in studying the physics of turbulent flows.

PACS numbers: 47.11.St, 47.45.-n, 47.61.-k

* zlguo@hust.edu.cn

I. INTRODUCTION

In the study of turbulent flows, the ultimate objective is to obtain accurate coarse-grained quantitative theories or models. However, experience over more than a century has shown it to be notoriously difficult [1]. Fortunately, the ever-increasing power of computers makes it possible to calculate relevant properties of turbulent flows by direct numerical simulation (DNS). Significant insight into turbulence physics has been gained from the DNS of some idealized flows that cannot be easily obtained in the laboratory [2–4]. The conventional DNS is based on the Navier-Stokes equations (NSEs), which are a set of second-order nonlinear partial-differential equations (PDE). However it is usually involute and computationally expensive to deal with the nonlinear and non-local convection term and pressure-gradient term in the NSEs [1]. Therefore, it is desirable to find an alternative numerical method for DNS which not only can accurately capture all the scales of turbulence, but is simpler and more efficient. Recently, Boltzmann equation based kinetic schemes have received particular attentions as alternative solvers to the NSEs due to some distinctive features. Different from the NSEs, the Boltzmann equation is a first-order linear PDE, and the nonlinearity locally resides in its collision term; both make such schemes to be easily realized and parallelized to have a high computational efficiency. It has been argued that the kinetic equation with local nonlinearity is more feasible to handle the discontinuities or unresolved flow regions [5]. Furthermore, the Boltzmann equation provides a theoretical foundation for the hydrodynamic description from the underlying microscopic physics, and describes the phenomenon of fluid flows in the statistical mechanics framework. This physical mechanism is inherently consistent with the physical process of the turbulent flows which are characterized by its statistical behavior [6]. Therefore, the kinetic schemes based on the Boltzmann equation have a great potential for DNS of turbulent flows [7].

In recent years, some kinetic schemes have been utilized to simulate turbulent flows, such as the lattice Boltzmann equation (LBE) methods [8–22] and the gas kinetic schemes [23–27]. Particularly, the LBE methods have been successfully applied to complex and multiscale flows due to its simplicity in formulation and versatility [28–31]. The potential of the LBE methods for DNS of the turbulent flows has been demonstrated shortly after its emergence by comparing with pseudo-spectral (PS) simulations of the decaying homogeneous isotropic turbulence (DHIT) [8, 9] and turbulence shear flows [10, 11]. An appealing feature of the LBE methods in turbulence simulations, as a scheme of second-order spatial accuracy,

is that it has very low numerical dissipation compared to the second-order conventional Computational Fluids Dynamics (CFD) methods [32]. It has been demonstrated that the larger numerical dissipation in second-order accurate conventional CFD translates into the greater resolution requirements [3].

Recently, starting from the Boltzmann equation, a discrete unified gas-kinetic scheme (DUGKS) has been proposed for flows in all Knudsen regimes [33, 34]. Although sharing a common kinetic origin, there are some distinctive differences between DUGKS and LBE methods. In the standard LBE, the phase space and time step are coupled due to the particle motion from one node to another one within a time step [31], but the DUGKS has no such a restriction and the time step is independently determined by Courant-Friedrichs-Lewy (CFL) condition [33]. In addition, the streaming process in LBE makes it difficult to be extended to non-uniform mesh, while the DUGKS can use arbitrary meshes [35]. Although some efforts have been made to release the close coupling between the mesh and discrete velocities [36–42], the decoupling also destroys the nice features of the standard LBE. For example, many of the existing finite volume (FV) LBE methods suffer from large numerical dissipation and poor numerical stability [40, 41]. More importantly, there are modeling difference in LBE and DUGKS in the treatment of particle evolution. In the LBE, the particle streaming and collision processes are splitted. But, these two processes are fully coupled in DUGKS. It has been demonstrated that such a strategy ensures a low numerical dissipation feature [43, 44]. It should be noted that although in some cases a finite-volume scheme can be identical to a finite-difference scheme, the DUGKS does not reduce to the standard LBE method generally, because the shift (streaming) operation in the LBE cannot be realized for some discrete populations in the FV framework (e.g., the diagonal populations in the D2Q9 model). Furthermore, in DUGKS the flux is evaluated by solving the evolution equation rather than interpolation. Therefore, the DUGKS would not be identical to the LBE. Consequently, these dynamic differences between the LBE and DUGKS methods determine the quality of solution in flow simulations. A comparative study of the LBE and DUGKS methods for laminar flows in the nearly incompressible limit has been made recently [45], which demonstrates that the DUGKS has the same accuracy as the LBE, but exhibits a superior numerical stability. The superiority of the DUGKS compared to the LBE methods for laminar flows motivates us to make a further comparative study of DUGKS and LBE methods for turbulent flows.

Our long term goal concentrates on providing some insights into the physics of complex

turbulent flows by using DUGKS as a DNS tool. At a first step, the validation of the DUGKS for simulating simple turbulent flows must be undertaken. The DHIT is one of such basic flows in turbulence study, and also a canonical case to validate a numerical scheme for DNS of turbulent flows. The objective of this work is to make a detailed comparison of the LBE and DUGKS methods by simulating the DHIT in a periodic box. To date, the pseudo-spectral (PS) method is well-established as the most accurate numerical tool for DNS of the DHIT. Therefore the DUGKS numerical results will be validated against those from the pseudo-spectral (PS) method. In addition, we use the LBE with the multiple relaxation time (MRT-LBE) collision model in this work due to its superiority to the single relaxation collision model [45]. The comparative study covers the following aspects of the simulated flows: (i) the instantaneous velocity and vorticity fields; (ii) the evolutions of kinetic energy, dissipation rate and enstrophy; (iii) the energy and the dissipation rate spectra; (iv) the evolutions of the Kolmogorov length scale and the Taylor micro-scale length; and (v) the evolutions of the averaged velocity-derivative skewness and flatness. Furthermore, DNS of the Kida flow is also performed by the LBE and DUGKS methods, and some comparisons are performed in terms of the vorticity, evolutions of the total kinetic energy, dissipation rate, enstrophy and Kolmogorov length scale, the longitudinal and transverse correlations, and the pressure-velocity correlations.

The remainder of this paper is organized as follows: in Sec. II, we provide a brief introduction of the DUGKS and MRT-LBE methods; Sec. III introduces the DHIT and Kida vortex flow, and the quantities to be computed; Sec. IV presents the numerical results followed by a summary of conclusions.

II. NUMERICAL METHODS

In this section, the essentials of DUGKS and MRT-LBE will be introduced briefly first. A more detailed description can be found in the references [13, 33].

A. The DUGKS method

The DUGKS is based on the BGK collision model [46], which begins with the model Boltzmann equation,

$$\frac{\partial f}{\partial t} + \boldsymbol{\xi} \cdot \nabla_x f = \Omega \equiv \frac{f^{eq} - f}{\tau}, \tag{1}$$

where $f = f(\boldsymbol{x}, \boldsymbol{\xi}, t)$ is the particle distribution function with particle velocity $\boldsymbol{\xi}$ at position $\boldsymbol{x}$ and time t, and f^{eq} is the Maxiwellian equilibrium distribution function,

$$f^{eq} = \frac{\rho}{(2\pi RT)^{D/2}} \exp\left(-\frac{(\boldsymbol{\xi} - \boldsymbol{u})^2}{2RT}\right), \tag{2}$$

where R is the gas constant, D is the spatial dimension, ρ is the density, $\boldsymbol{u}$ is the fluid velocity, and T is the temperature. It should be noted that the dimensions of f and f^{eq} are both $kg/\left[m^D \cdot (m/s)^D\right]$. For incompressible flow (i.e., when the Mach number Ma is small), the Maxwellian distribution can be approximated by its Taylor expansion around zero particle velocity. As a result, the expanded equilibrium distribution function becomes

$$f^{eq} = \frac{\rho}{(2\pi RT)^{D/2}} \exp\left(-\frac{|\,\boldsymbol{\xi}\,|^2}{2RT}\right)\left[1 + \frac{\boldsymbol{\xi}\cdot\boldsymbol{u}}{RT} + \frac{(\boldsymbol{\xi}\cdot\boldsymbol{u})^2}{2(RT)^2} - \frac{|\,\boldsymbol{u}\,|^2}{2RT}\right]. \tag{3}$$

In order to obtain the correct NSEs in the limit of low Mach number, the discrete velocity set should be chosen so that the following quadratures of the expanded equilibrium distribution function hold exactly

$$\int \boldsymbol{\xi}^k f^{eq} d\boldsymbol{\xi} = \sum_i \omega_i \boldsymbol{\xi}_i^k f^{eq}(\boldsymbol{\xi}_i), \quad 0 \le k \le 3 \tag{4}$$

where ω_i and $\boldsymbol{\xi}_i$ are the weights and points of the numerical quadrature rule. Based on the formulation of Eq. (3), it is natural to choose a Guassian quadrature with $\omega_i = W_i(2\pi RT)^{D/2}\exp\left(\frac{|\xi_i|^2}{2RT}\right)$, in which W_i is the weight coefficient corresponding to the particle velocity $\boldsymbol{\xi}_i$.

In the present study, we use the nineteen velocities in three dimensions, i.e., the D3Q19 model, for both the DUGKS and LBE, where

$$\boldsymbol{\xi}_i = \begin{cases} (0,0) & i = 0 \\ (\pm 1, 0, 0)\, c, (0, \pm 1, 0)\, c, (0, 0, \pm 1)\, c & i = 1 - 6, \\ (\pm 1, \pm 1, 0)\, c, (\pm 1, 0, \pm 1)\, c, (0, \pm 1, \pm 1)\, c & i = 7 - 18, \end{cases} \tag{5}$$

where $c = \sqrt{3RT}$, and the corresponding weight coefficients are $W_0 = 1/3$, $W_{1,\ldots,6} = 1/18$ and $W_{7,\ldots,18} = 1/36$.

Once the quadrature rule is chosen, we can define a discrete distribution function, $f_i(\boldsymbol{x}, t) = \omega_i f(\boldsymbol{x}, \boldsymbol{\xi}_i, t)$, which satisfies the following equation

$$\frac{\partial f_i}{\partial t} + \boldsymbol{\xi}_i \cdot \nabla_x f_i = \Omega_i \equiv \frac{f_i^{eq} - f_i}{\tau}. \tag{6}$$

where $f_i^{eq} = \omega_i f^{eq}(\boldsymbol{\xi}_i)$ is the discrete expanded equilibrium distribution function that can be written as

$$f_i^{eq} = W_i \left[\delta\rho + \rho_0 \left(\frac{\boldsymbol{\xi}_i \cdot \boldsymbol{u}}{RT} + \frac{(\boldsymbol{\xi}_i \cdot \boldsymbol{u})^2}{2(RT)^2} - \frac{|\,\boldsymbol{u}\,|^2}{2RT} \right) \right], \tag{7}$$

where the density has been expressed as $\rho = \delta\rho + \rho_0$, in which $\delta\rho$ is the density fluctuation, ρ_0 is the constant mean density of the fluid which is usually set to be 1. It should be emphasized that with the discrete velocity set, the dimensions of f_i and f_i^{eq} are both kg/m^D. Then, the fluid density and velocity can be obtained from the discrete distribution function,

$$\rho = \rho_0 + \delta\rho, \quad \delta\rho = \sum_i f_i, \quad \rho_0 \boldsymbol{u} = \sum_i \boldsymbol{\xi}_i f_i \tag{8}$$

The DUGKS is a finite-volume scheme in which the computational domain is divided into a set of control volumes. Then integrating Eq. (6) over a control volume V_j centered at $\boldsymbol{x}_j$ from t_n to t_{n+1} (the time step $\Delta t = t_{n+1} - t_n$ is assumed to be a constant in the present work), and using the midpoint rule for the integration of the flux term at the cell boundary and trapezoidal rule for the collision term inside each cell [33], we can get the evolution equation of DUGKS

$$\tilde{f}_{i,j}^{n+1} = \tilde{f}_{i,j}^{+,n} - \frac{\Delta t}{|V_j|} F_i^{n+1/2}, \tag{9}$$

where

$$F_i^{n+1/2} = \int_{\partial V_j} (\boldsymbol{\xi}_i \cdot \boldsymbol{n})\, f_i\left(\boldsymbol{x}, t_{n+1/2}\right) d\boldsymbol{S}, \tag{10}$$

is the flux across the cell interface, and

$$\tilde{f}_i = f_i - \frac{\Delta t}{2}\Omega_i, \;\; \tilde{f}_i^{+} = f_i + \frac{\Delta t}{2}\Omega_i. \tag{11}$$

Based on the compatibility condition and the relationship between f_i and $\tilde{f}_i$, the density ρ and velocity $\boldsymbol{u}$ can be computed by

$$\rho = \rho_0 + \delta\rho, \quad \delta\rho = \sum_i \tilde{f}_i, \quad \rho_0 \boldsymbol{u} = \sum_i \boldsymbol{\xi}_i \tilde{f}_i. \tag{12}$$

The key ingredient in updating $\tilde{f}_i$ is to evaluate the interface flux $F_i^{n+1/2}$, which is solely determined by the distribution function $f_i(\boldsymbol{x}, t_{n+1/2})$ there. In DUGKS, after integrating Eq. (6) along a particle path within a half time step ($h = \Delta t/2$), the evaluation of the distribution function $f_i(\boldsymbol{x}, t_{n+1/2})$ at the cell interface can be traced back to the interior of neighboring cells,

$$\bar{f}_i(\boldsymbol{x}_b, t_n + h) = \bar{f}_i^{+}(\boldsymbol{x}_b, t_n) - h\boldsymbol{\xi}_i \cdot \boldsymbol{\sigma}_b, \tag{13}$$

where

$$\bar{f}_i = f_i - \frac{h}{2}\Omega_i, \;\; \bar{f}_i^{+} = f_i + \frac{h}{2}\Omega_i, \tag{14}$$

$\bar{f}_i^{+}(\boldsymbol{x}_b, t_n)$ and the gradient $\boldsymbol{\sigma}_b = \nabla \bar{f}_i^{+}(\boldsymbol{x}_b, t_n)$ can be approximated by linear interpolation. For example, in the one dimensional case, the reconstructions become

$$\bar{f}_i^{+}(x_{j+1/2}, t_n) = \bar{f}_i^{+}(x_j, t_n) + \sigma_{j+1/2}(x_{j+1/2} - x_j), \tag{15}$$

where

$$\sigma_{j+1/2} = \frac{\bar{f}_i^{+}(x_{j+1}, t_n) - \bar{f}_i^{+}(x_j, t_n)}{x_{j+1} - x_j}. \tag{16}$$

Note that the particle collision effect from t_n to t_{n+1} is included in the above reconstruction of the interface distribution function. This is the key for the success of the DUGKS. Owing to the coupled treatment of the particle collision and transport process in the reconstruction of the distribution function at cell interfaces, DUGKS is a self-adaptive scheme for different flow regimes. It has been shown in Ref. [33] that the reconstructed distribution function reduces to the Chapman-Enskog one approximation at the Navier-Stokes level in the continuum limit, and to the free-transport approximation in the free-molecular limit.

Based on the compatibility condition and the relationship between f_i and $\bar{f}_i$, the density ρ and velocity $\boldsymbol{u}$ at the cell interface can be obtained,

$$\rho = \rho_0 + \delta\rho, \quad \delta\rho = \sum_i \bar{f}_i, \quad \rho_0 \boldsymbol{u} = \sum_i \boldsymbol{\xi}_i \bar{f}_i \tag{17}$$

from which the equilibrium distribution function $f_i^{eq}(\boldsymbol{x}_b, t^n + h)$ at the cell interface can be obtained. Therefore, based on Eq. (14) and the obtained equilibrium state, the real distribution function at the cell interface can be determined from $\bar{f}_i$ as,

$$f_i(\boldsymbol{x}_b, t_n + h) = \frac{2\tau}{2\tau + h}\bar{f}_i(\boldsymbol{x}_b, t_n + h) + \frac{h}{2\tau + h} f_i^{eq}(\boldsymbol{x}_b, t_n + h), \tag{18}$$

from which the interface flux term can be evaluated.

In computation, we only need to follow the evolution of $\tilde{f}_i$ in Eq. (9). The required variables for its evolution are determined by [33]

$$\bar{f}_i^{+} = \frac{2\tau - h}{2\tau + \Delta t}\tilde{f}_i + \frac{3h}{2\tau + \Delta t} f_i^{eq}, \tag{19}$$

$$\tilde{f}_i^{+} = \frac{4}{3}\bar{f}_i^{+} - \frac{1}{3}\tilde{f}_i. \tag{20}$$

B. The MRT-LBE method

In this work, we use the LBE with multiple-relaxation time collision model (MRT-LBE) and the D3Q19 discrete velocity sets. The evolution equation of the MRT-LBE is

$$\mathbf{f}(\boldsymbol{x}+\xi_i\Delta t, t_n+\Delta t) = \mathbf{f}(\boldsymbol{x}, t_n) - \mathbf{M}^{-1}\mathbf{S}\left[\mathbf{m}(\boldsymbol{x},t) - \mathbf{m}^{eq}(\boldsymbol{x},t)\right], \tag{21}$$

where $\mathbf{M}$ is an orthogonal transformation matrix converting the distribution function $\mathbf{f}$ from discrete velocity space to the moment space $\mathbf{m}$, in which the collision relaxation is performed.

The basic idea of MRT-LBE is that the streaming sub-step is handled in the microscopic lattice-velocity space but the collision sub-step is performed in the moment space. The transformation between the microscopic velocity space and the moment space is carried out by matrix operations as $\mathbf{m} = \mathbf{M}\cdot\mathbf{f},\ \mathbf{f} = \mathbf{M^{-1}}\cdot\mathbf{m}$. The diagonal relaxation matrix $\mathbf{S}$ specifies the relaxation rates for the non-conserved moments.

The macroscopic hydrodynamic variables, including the density ρ and momentum, are obtained from the moments of the mesoscopic distribution function $\mathbf{f}$. In the nearly incompressible formulation [47]

$$\rho = \rho_0 + \delta\rho, \quad \rho_0 = 1; \quad \delta\rho = \sum_i f_i, \quad \rho_0\boldsymbol{u} = (j_x, j_y, j_z)^T = \sum_i \boldsymbol{\xi}_i f_i. \tag{22}$$

For the D3Q19 velocity model, the corresponding 19 orthogonal moments

$$\mathbf{m} = (\delta\rho, e, \varepsilon, j_x, q_x, j_y, q_y, j_z, q_z, 3p_{xx}, 3\pi_{xx}, p_{ww}, \pi_{ww}, p_{xy}, p_{yz}, p_{xz}, m_x, m_y, m_z)^T$$

are defined through the element of the transformation matrix (each subscript runs from 0 to 18) as

$$\begin{aligned}
&M_{0,\alpha} = ||\xi_\alpha||^0, \quad M_{1,\alpha} = 19||\xi_\alpha||^2 - 30, \quad M_{2,\alpha} = \left(21||\xi_\alpha||^4 - 53||\xi_\alpha||^2 + 24\right)/2 \\
&M_{3,\alpha} = \xi_{\alpha x}, \quad M_{5,\alpha} = \xi_{\alpha y}, \quad M_{7,\alpha} = \xi_{\alpha z}, \\
&M_{4,\alpha} = \left(5||\xi_\alpha||^2 - 9\right)\xi_{\alpha x}, \quad M_{6,\alpha} = \left(5||\xi_\alpha||^2 - 9\right)\xi_{\alpha y}, \quad M_{8,\alpha} = \left(5||\xi_\alpha||^2 - 9\right)\xi_{\alpha z}, \\
&M_{9,\alpha} = 3\xi_{\alpha x}^2 - ||\xi_\alpha||^2, \quad M_{11,\alpha} = \xi_{\alpha y}^2 - \xi_{\alpha z}^2, \\
&M_{13,\alpha} = \xi_{\alpha x}\xi_{\alpha y}, \quad M_{14,\alpha} = \xi_{\alpha y}\xi_{\alpha z}, \quad M_{15,\alpha} = \xi_{\alpha x}\xi_{\alpha z}, \\
&M_{10,\alpha} = \left(3||\xi_\alpha||^2 - 5\right)\left(3\xi_{\alpha x}^2 - ||\xi_\alpha||^2\right), \quad M_{12,\alpha} = \left(3||\xi_\alpha||^2 - 5\right)\left(\xi_{\alpha y}^2 - \xi_{\alpha z}^2\right), \\
&M_{16,\alpha} = \left(\xi_{\alpha y}^2 - \xi_{\alpha z}^2\right)\xi_{\alpha x}, \quad M_{17,\alpha} = \left(\xi_{\alpha z}^2 - \xi_{\alpha x}^2\right)\xi_{\alpha y}, \quad M_{18,\alpha} = \left(\xi_{\alpha x}^2 - \xi_{\alpha y}^2\right)\xi_{\alpha z}.
\end{aligned}$$

The equilibrium moments are defined as

$$
\begin{aligned}
&\widetilde{\rho}^{(eq)} = \widetilde{\rho} = \delta\rho, \quad e^{(eq)} = -11\delta\rho + \frac{19}{\rho_0}\left(j_x^2 + j_y^2 + j_z^2\right), \quad \varepsilon^{(eq)} = \omega_\varepsilon \delta\rho + \frac{\omega_{\varepsilon j}}{\rho_0}\left(j_x^2 + j_y^2 + j_z^2\right), \\
&j_x^{(eq)} = j_x = \rho_0 u_x, \quad j_y^{(eq)} = j_y = \rho_0 u_y, \quad j_z^{(eq)} = j_z = \rho_0 u_z, \\
&q_x^{(eq)} = -\frac{2}{3} j_x, \quad q_y^{(eq)} = -\frac{2}{3} j_y, \quad q_z^{(eq)} = -\frac{2}{3} j_z, \\
&p_{xx}^{(eq)} = \frac{1}{3\rho_0}\left[2j_x^2 - \left(j_y^2 + j_z^2\right)\right], \quad p_{ww}^{(eq)} = \frac{1}{\rho_0}\left[j_y^2 - j_z^2\right], \\
&p_{xy}^{(eq)} = \frac{1}{\rho_0} j_x j_y, \quad p_{yz}^{(eq)} = \frac{1}{\rho_0} j_y j_z, \quad p_{xz}^{(eq)} = \frac{1}{\rho_0} j_x j_z, \\
&\pi_{xx}^{(eq)} = \omega_{xx} p_{xx}^{(eq)}, \quad \pi_{ww}^{(eq)} = \omega_{xx} p_{ww}^{(eq)}, \\
&m_x^{(eq)} = m_y^{(eq)} = m_z^{(eq)} = 0,
\end{aligned}
$$

with the following relaxation parameters

$$
\mathbf{S} = \mathrm{diag}\left(0, s_1, s_2, 0, s_4, 0, s_4, 0, s_4, s_9, s_{10}, s_9, s_{10}, s_{13}, s_{13}, s_{13}, s_{16}, s_{16}, s_{16}\right).
$$

The kinematic viscosity ν and bulk viscosity ζ are related to the relaxation rates s_9 and s_1, respectively, where

$$
\nu = \frac{1}{3}\left(\frac{1}{s_9} - \frac{1}{2}\right) c\Delta x, \tag{23}
$$

$$
\zeta = \frac{5 - 9c_s^2}{9}\left(\frac{1}{s_1} - \frac{1}{2}\right) c\Delta x, \tag{24}
$$

where $c_s^2 = RT$ is the speed of sound.

It is noted that some of the relaxation parameters do not affect the simulated flow, but may affect the numerical stability of the code. Specifically, s_1 determines the bulk viscosity which could absorb low-amplitude acoustic oscillations.

III. DECAYING TURBULENT FLOWS

A. Decaying Homogeneous Isotropic Turbulence

The DHIT in a three-dimensional box with periodic boundary conditions in all three directions is a standard test case to validate numerical scheme for DNS. At the initial time, a random flow field is introduced with the kinetic energy contained only in the large eddies (i.e., at low wave numbers). This initial flow is unstable and large eddies will break up, transferring their energy successively to smaller and smaller eddies with high wave numbers until the eddy scale is sufficiently small, in which the eddy motions are stable and the

viscosity is effective in dissipating the kinetic energy. After some time, a realistic DHIT will develop with some larger eddies supply kinetic energy for smaller eddies and the viscous action controls the size of the small eddies.

In the present work, the incompressible initial velocity field $\boldsymbol{u}_0$ ($\nabla \cdot \boldsymbol{u}_0 = 0$) is specified by a Gaussian field with a prescribed kinetic energy spectrum [17]:

$$E_0(k) := E(k, t = 0) = Ak^4 e^{-0.14k^2}, \qquad k \in [k_{min}, k_{max}], \tag{25}$$

where k is the wavenumber, the magnitude A and the range of the initial energy spectrum $[k_{min}, k_{max}]$ determines the total initial kinetic energy K_0 in the simulation. The kinetic energy K, enstrophy, dissipation rate ϵ are respectively given by

$$K(t) = \int E(\boldsymbol{k}, t)d\boldsymbol{k}, \quad \Omega(t) = \int k^2 E(\boldsymbol{k}, t)d\boldsymbol{k}, \quad \epsilon(t) = 2\nu\Omega(t), \tag{26}$$

where ν is the kinematic viscosity, and

$$E(\boldsymbol{k}, t) = \frac{1}{2}\hat{\boldsymbol{u}}(\boldsymbol{k}, t)\hat{\boldsymbol{u}}^*(\boldsymbol{k}, t), \tag{27}$$

where $\hat{\boldsymbol{u}}$ and $\hat{\boldsymbol{u}}^*$ are velocity and its complex conjugate in the spectral space. The DHIT is typically characterized by the Taylor microscale Reynolds number

$$Re_\lambda = \frac{u'\lambda}{\nu} \tag{28}$$

where u' is the root mean squared (rms) value of the turbulent fluctuating velocity $\boldsymbol{u}$ in a given spatial direction and is defined by

$$u' = \frac{1}{\sqrt{3}}\sqrt{\langle \boldsymbol{u} \cdot \boldsymbol{u} \rangle}, \tag{29}$$

here $\langle \cdot \rangle$ designates the volume average; λ is the transverse Taylor microscale length

$$\lambda = \sqrt{\frac{15\nu}{\epsilon}}u'. \tag{30}$$

The other statistical quantities of interest are as follows:

$$\eta = \sqrt[4]{\nu^3/\epsilon} \tag{31a}$$

$$D(k, t) = 2\nu k^2 E(k, t), \tag{31b}$$

$$S(t) = \frac{\langle(\partial_x u)^3\rangle + \langle(\partial_y v)^3\rangle + \langle(\partial_z w)^3\rangle}{3\left[\langle(\partial_x u)^2\rangle^{3/2} + \langle(\partial_y v)^2\rangle^{3/2} + \langle(\partial_z w)^2\rangle^{3/2}\right]} \tag{31c}$$

$$F(t) = \frac{\langle(\partial_x u)^4\rangle + \langle(\partial_y v)^4\rangle + \langle(\partial_z w)^4\rangle}{3\left[\langle(\partial_x u)^2\rangle^2 + \langle(\partial_y v)^2\rangle^2 + \langle(\partial_z w)^2\rangle^2\right]} \tag{31d}$$

where η is the Kolmogorov length and $D(k, t)$ is the energy dissipation rate spectrum; $S(t)$ and $F(t)$ are the velocity-derivative skewness and flatness averaged over three directions, respectively.

B. Kida vortex flow

The Kida vortex flow is another decaying turbulent flow which has been well studied by various LBE methods [20–22, 48]. The flow evolves from a simple deterministic and symmetric initial condition to a state which resembles a fully developed turbulent flow. The initial conditions for the flow field are given by

$$u(x,y,z) = U_0 \sin x \ (\cos 3y \cos z - \cos y \cos 3z \ ) \tag{32a}$$

$$v(x,y,z) = U_0 \sin y \ (\cos 3z \cos x \ - \cos z \cos 3x \ ) \tag{32b}$$

$$w(x,y,z) = U_0 \sin z \ (\cos 3x \cos y \ - \cos x \cos 3y \ ), \tag{32c}$$

where $x, y, z \in [0, 2\pi]$, U_0 is the initial velocity, and the periodic boundary conditions are imposed in all directions.

In addition to one point statistics, we will also compare some two point statistics for the Kida vortex flow, including the longitudinal correlation function [20, 21]

$$\rho_{11}(r) = \frac{\langle u(x,y,z)u(x+r,y,z)\rangle}{\langle u(x,y,z)u(x,y,z)\rangle}, \tag{33}$$

transverse correlation functions

$$\rho_{22}(r) = \frac{\langle v(x,y,z)v(x+r,y,z)\rangle}{\langle v(x,y,z)v(x,y,z)\rangle}, \tag{34a}$$

$$\rho_{33}(r) = \frac{\langle w(x,y,z)w(x+r,y,z)\rangle}{\langle w(x,y,z)w(x,y,z)\rangle}, \tag{34b}$$

and the pressure-velocity correlation functions [49]

$$PU(r) = \langle |p(x,y,z)u(x,y,z) - p(x+r,y,z)u(x+r,y,z)| \rangle, \tag{35a}$$

$$PV(r) = \langle |p(x,y,z)v(x,y,z) - p(x+r,y,z)v(x+r,y,z)| \rangle, \tag{35b}$$

$$PW(r) = \langle |p(x,y,z)w(x,y,z) - p(x+r,y,z)w(x+r,y,z)| \rangle. \tag{35c}$$

IV. NUMERICAL RESULTS

A. Decaying Homogeneous Isotropic Turbulence

1. *Initial conditions*

We perform the simulations of DHIT in a periodic box with the domain size L^3 using the LBE, DUGKS and PS methods. The focus is on the comparison of LBE and DUGKS

results with those from the PS method which is used as a benchmark due to its superior spatial accuracy. The PS method is same as in Ref. [17]. The units of LBE and DUGKS are converted back to the spectral units to allow for a direct comparison. The conversion requires a velocity scale V_s which is the ratio of the fluid velocity magnitude in LBE or DUGKS units to the velocity magnitude in spectral units.

In the PS simulation, the domain size is set to be $L^3 = (2\pi)^3$; for the initial energy spectrum $E_0(k)$ given by Eq. (25), we set $A = 1.7414 \times 10^{-2}$, $k_{min} = 3$ and $k_{max} = 8$ such that the initial kinetic energy is $K_0 = 0.9241$ and the rms velocity is $u_0' = 0.7849$.

In the LBE and DUGKS simulations, we set the domain size $L^3 = N^3$, where N is the number of the cells or lattices in each spatial direction. In addition, we must ensure that the local Mach number (Ma) is small enough so that the flow is nearly incompressible, which can be met by choosing a suitable V_s. In the simulations, we chose velocity scale $V_s = 0.0408$ which leads to the initial kinetic energy $K_0 = 1.5383 \times 10^{-3}$, the corresponding initial rms velocity $u_0' = 0.0320$ and maximum velocity magnitude $\|\boldsymbol{u}_0\|_{max} = 0.1660$ so that the maximum Mach number $\text{Ma} = \|\boldsymbol{u}_0\|_{max}/c_s = 0.2875$, here $c_s = \sqrt{RT}$, $RT = 1/3$. The initial velocity field and parameters used in the LBE and DUGKS simulations are identical except the time step size Δt. In LBE method, the time step size $\Delta t = \Delta x = 1$ in LBE units, while in DUGKS it is solely determined by the CFL condition, i.e., $\Delta t = \gamma \Delta x_{min}/\sqrt{2}c$, where γ is the CFL number and Δx_{min} is the minimum grid spacing and $\sqrt{2}c$ is the maximum discrete particle speed in D3Q19. In the DUGKS simulations, we set $\gamma = 0.7071$ such that the time step $\Delta t = 0.5$ for convenient comparison. Moreover, for the MRT-LBE, the specific parameters are set to be $\omega_\varepsilon = \omega_{xx} = 0$, $\omega_{\varepsilon j} = -475/63$, $s_2 = s_{10} = 1.4$, $s_9 = s_{13} = \Delta t/(3\nu + 0.5\Delta t)$, $s_1 = 1.19, s_4 = 1.2$, and $s_{16} = 1.98$ [13].

TABLE I: Parameters used in the LBE, DUGKS and PS simulations.

method	L	N	K_0	u_0'	ν
PS128	2π	128	0.9241	0.7849	1.4933×10^{-2}
LBE128	128	128	1.5383×10^{-3}	0.0320	1.2395×10^{-2}
DUGKS128	128	128	1.5383×10^{-3}	0.0320	1.2395×10^{-2}
PS256	2π	256	0.9241	0.7849	1.4933×10^{-2}
LBE256	256	256	1.5383×10^{-3}	0.0320	2.4790×10^{-2}
DUGKS256	256	256	1.5383×10^{-3}	0.0320	2.4790×10^{-2}

Table I summarizes the parameters used in the simulations with these three methods. Two mesh resolutions are considered in the simulations. In order to fix the initial Taylor microscale Reynolds number $\mathrm{Re}_\lambda = 26.06$, in the PS simulation we set the kinematic viscosity $\nu = 1.4933 \times 10^{-2}$ for both resolutions, while in the LBE and DUGKS simulations, we set the viscosity $\nu = 1.2395 \times 10^{-2}$ and 2.4790×10^{-2} for the mesh resolutions of 128^3 and 256^3, respectively. It should be noted that the flow is over resolved in the PS simulations as the minimum spatial resolution parameter $k_{max}\eta$ is larger than 2.07 at 128^3 and 4.15 at 256^3, respectively, where k_{max} is the maximum resolved wave number [50]. This implies that the results from the PS simulations at the two grid resolutions would be identical. The non-dimensional time step size, normalized by the turbulence eddy turnover time $t_0 = K_0/\epsilon_0$, is $\Delta t' = \Delta t \epsilon_0 / K_0$.

With the initial velocity field $\boldsymbol{u}_0$, the initial pressure p_0 is obtained by solving the Poisson equation in the spectral space for the PS method. As for the LBE and DUGKS methods, besides the pressure p_0, herein related to the density fluctuation by equation of the state, a consistent initial distribution function including the non-equilibrium part should be specified, which is achieved by using the iterative procedure described in [51].

2. Instantaneous velocity and vorticity fields

We compare the instantaneous velocity and vorticity magnitude obtained by LBE and DUGKS methods with those from PS simulation on the xy plane at $z = L/2$. The vorticity fields for all three methods are first computed in the spectral space, $\tilde{\omega} = i\boldsymbol{k} \times \tilde{\boldsymbol{u}}$, and then $\tilde{\boldsymbol{\omega}}$ is transferred back to the physical space using inverse fast Fourier translation (FFT).

Figure 1 shows the contours of normalized velocity magnitude $\|\boldsymbol{u}\|/u_0'$ and vorticity magnitude $\|\boldsymbol{\omega}\|L/u_0'$ at different non-dimensional times $t' = 0, 1.21, 6.08$ and 12.16 on a mesh of $N^3 = 128^3$. As shown in Figs. 1a and 1b, these three methods have the identical initial fields with many large eddies; then small scale eddies are produced by vortex stretching as shown in Figs. 1c and 1d; in the end, as shown in Figs. 1g and 1h, the small scale eddies are dissipated by viscous actions. As shown in these figures, although the fields predicted by the LBE and DUGKS methods are similar to each other, and very close to those from the PS simulation in terms of vortex shapes and locations, the discrepancy between the both kinetic methods and the PS method is still visible and increases over time.

We also conduct the simulations on a finer mesh of 256^3 at $\mathrm{Re}_\lambda = 26.06$. As shown in

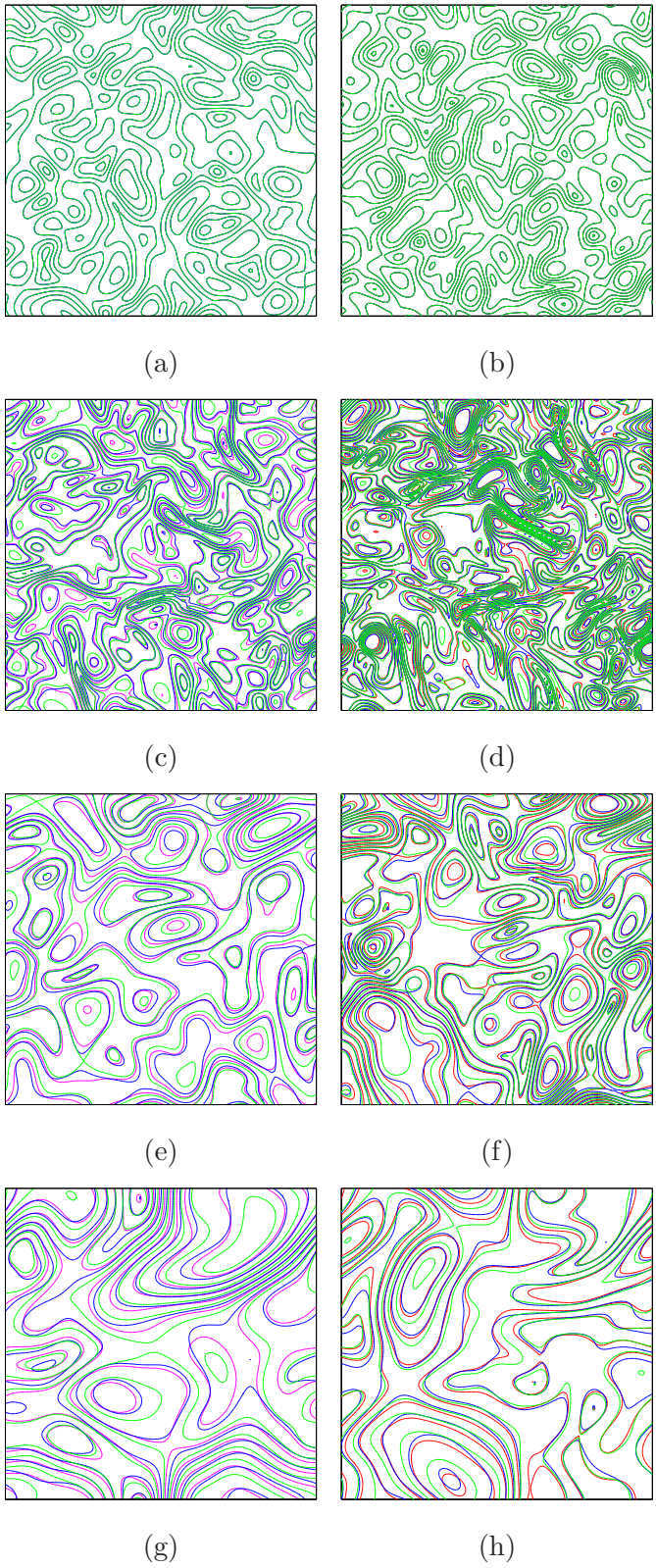

FIG. 1: Contours of normalized velocity magnitude $\|\boldsymbol{u}\|/u_0'$ (left column) and normalized vorticity magnitude $\|\boldsymbol{\omega}\|L/u_0'$ (right column) on the xy plane at $z = L/2$ at time $t' = 0, 1.21, 6.08$ and 12.16 (from top to bottom) with $N^3 = 128^3$. The solid red, green and blue lines denote results of the PS, LBE and DUGKS, respectively.

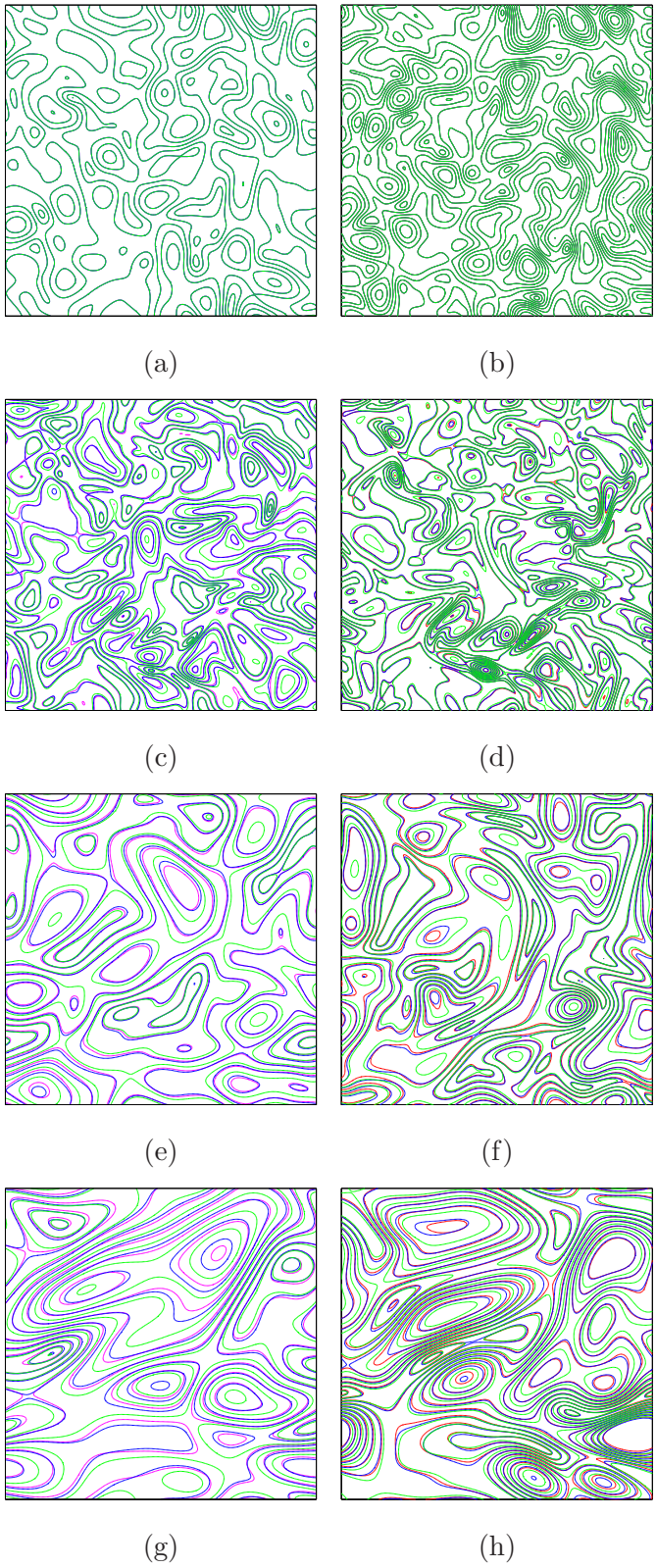

FIG. 2: Contours of normalized velocity magnitude $\|\boldsymbol{u}\|/u_0'$ (left column) and normalized vorticity magnitude $\|\boldsymbol{\omega}\|L/u_0'$ (right column) on the xy plane at $z = L/2$ at time $t' = 0, 1.21, 6.08$ and 12.16 (from top to bottom) with $N^3 = 256^3$. The solid red, green and blue lines denote results of the PS, LBE and DUGKS, respectively.

Fig. 2, again the velocity magnitude (left column) and vorticity magnitude (right column) obtained from LBE and DUGKS methods are in good agreement with those from PS method. It can be seen that both kinetic methods with the fine resolution give much better prediction than those with the coarse one.

3. Statistical quantities

In this subsection, we compare some key statistical quantities, including both the low and high order statistical quantities, obtained by the LBE and DUGKS methods with those from the PS method. The simulations of these three methods are performed on both $N^3 = 128^3$ and 256^3 mesh resolutions.

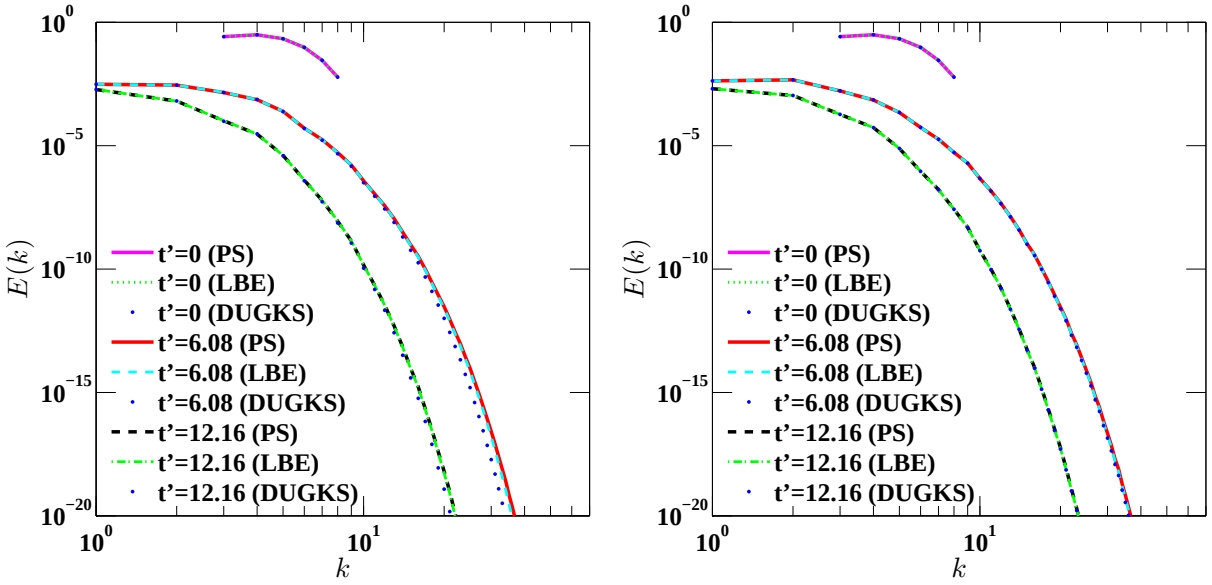

(a) (b)

FIG. 3: The energy spectra $E(k,t)$ with different mesh resolutions of (a) $N^3 = 128^3$ and (b) $N^3 = 256^3$ at $\mathrm{Re}_\lambda = 26.06$.

We first compare the energy spectra ($E(k)$) and dissipation spectra ($D(k)$) at $t' = 0, 6.08$ and 12.16. As shown in Figs. 3a and 4a, the results computed by the LBE and DUGKS agree well with those from the PS counterparts. It should be noted that although there are a little deviations in the high wavenumber region for the results of DUGKS on the mesh of 128^3, the values of the both spectra have decreased to the 10^{-10} magnitude of the maximum initial value, which will not cause significant deviations on the integral quantities,

such as the normalized kinetic energy K/K_0 and dissipation rate ϵ/ϵ_0 shown in Fig. 7a. This discrepancy may be caused by the numerical dissipation, which is proportional to the mesh size. Therefore we can refine the mesh resolution to reduce the numerical dissipation. As expected, as shown in Figs. 3b and 4b, with mesh resolution of 256^3 the results of DUGKS show no visible difference with those from the LBE and PS simulations. We also compute the difference of the spectra between both kinetic methods and the PS method, which is defined by

$$\Delta S(k,t') = \|S(k,t') - S_p(k,t')\|, \tag{36}$$

where S denotes the results of energy spectra or dissipation rate spectra, and S_p represents the results from the PS simulations. Figures 5 and 6 respectively show the differences of energy spectra $\Delta E(k,t')$ and dissipation rate spectra $\Delta D(k,t')$ on both meshes. We observe that with the mesh of 128^3, the results obtained by LBE is slightly better than those from the DUGKS when compared with the PS results, but there is no visible difference when both methods used the fine mesh of 256^3. These results indicate that the dissipation of the DUGKS is slightly larger than the LBE method, though both LBE and DUGKS methods have low numerical dissipation.

Secondly, we compare the evolutions of normalized kinetic energy $K(t)/K_0$ and dissipa-

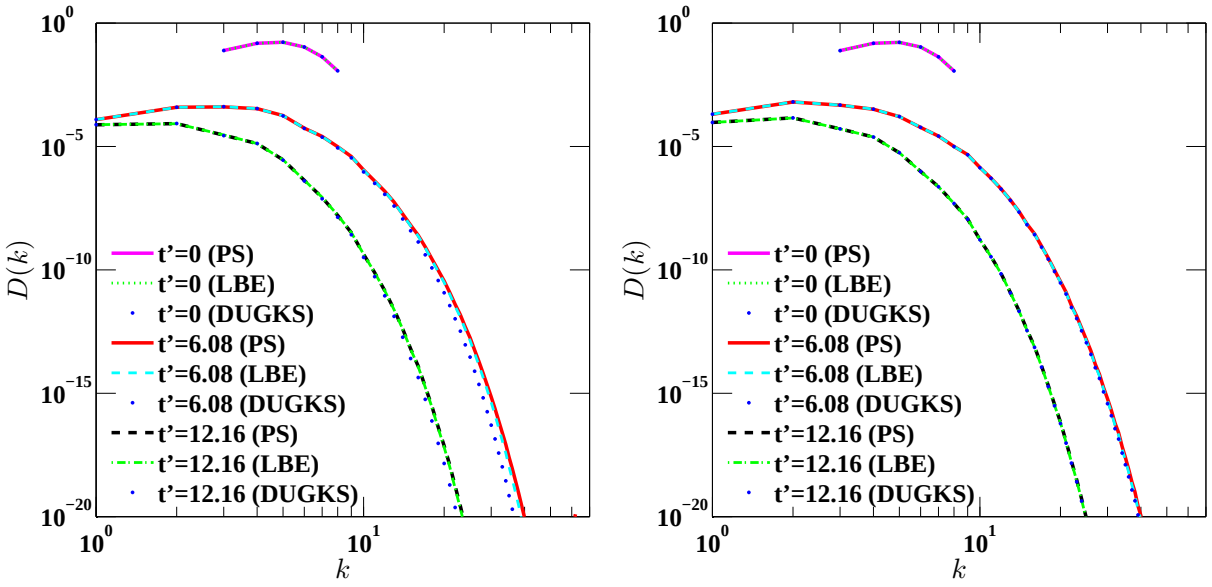

FIG. 4: The dissipation rate spectra $D(k,t)$ with different mesh resolutions of (a) $N^3 = 128^3$ and (b) $N^3 = 256^3$ at $\mathrm{Re}_\lambda = 26.06$.

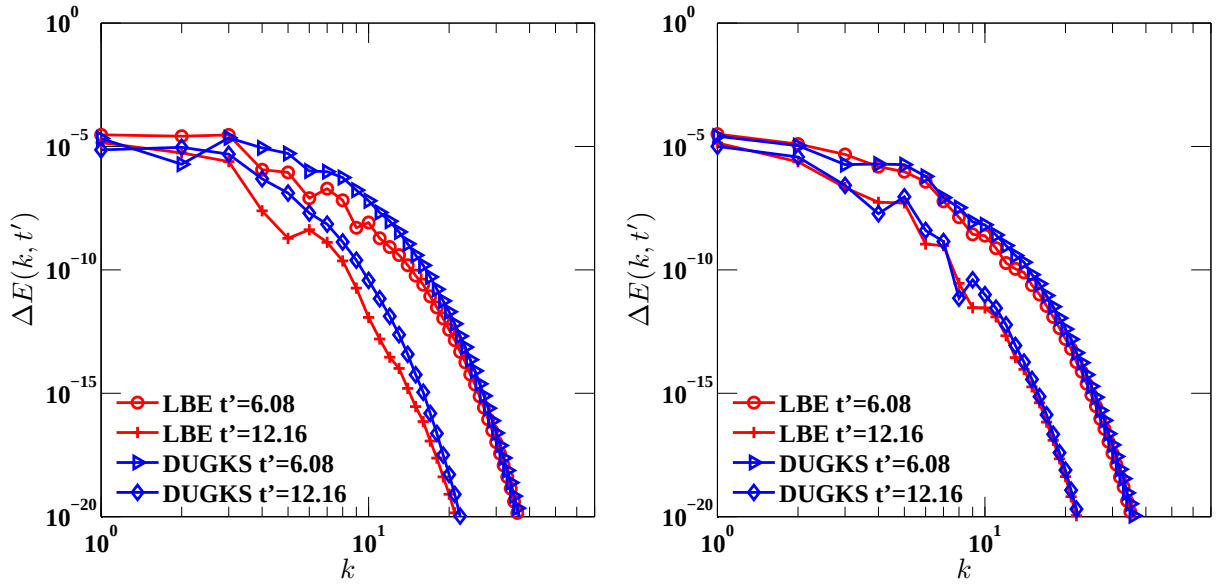

FIG. 5: The energy spectra difference $\Delta E(k,t')$ with different mesh resolutions of (a) $N^3 = 128^3$ and (b) $N^3 = 256^3$ at $\mathrm{Re}_\lambda = 26.06$.

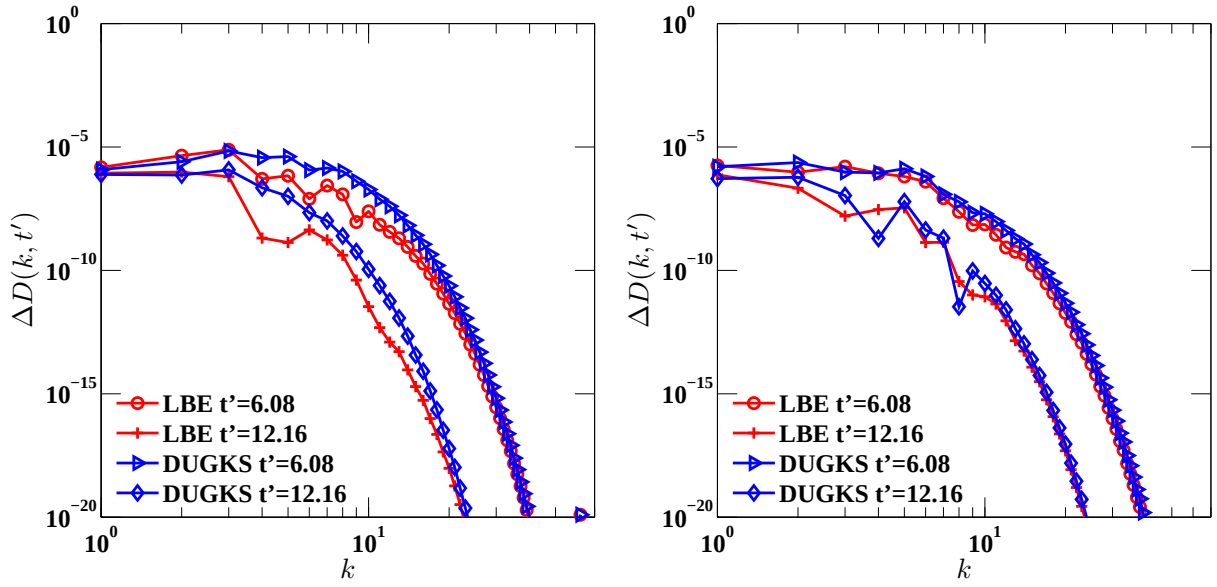

FIG. 6: The dissipation rate spectra difference $\Delta D(k,t)$ with different mesh resolutions of (a) $N^3 = 128^3$ and (b) $N^3 = 256^3$ at $\mathrm{Re}_\lambda = 26.06$.

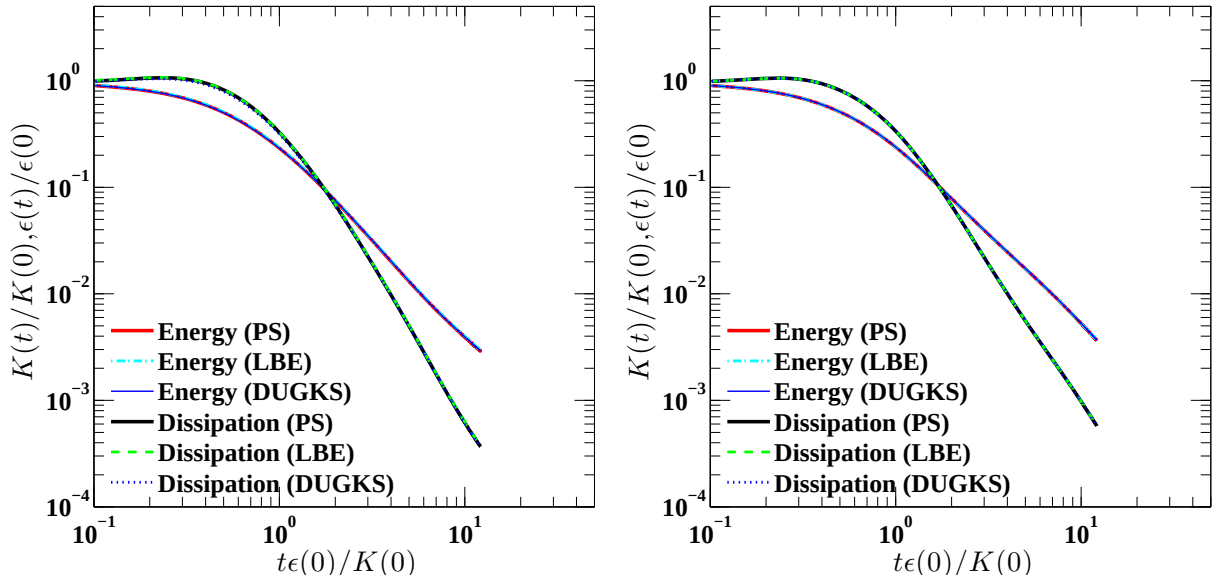

(a) (b)

FIG. 7: Evolutions of the normalized total kinetic energy $K(t)/K_0$ and the normalized dissipation rate $\epsilon(t)/\epsilon_0$ with different mesh resolutions of (a) $N^3 = 128^3$ and (b) $N^3 = 256^3$ at $\mathrm{Re}_\lambda = 26.06$.

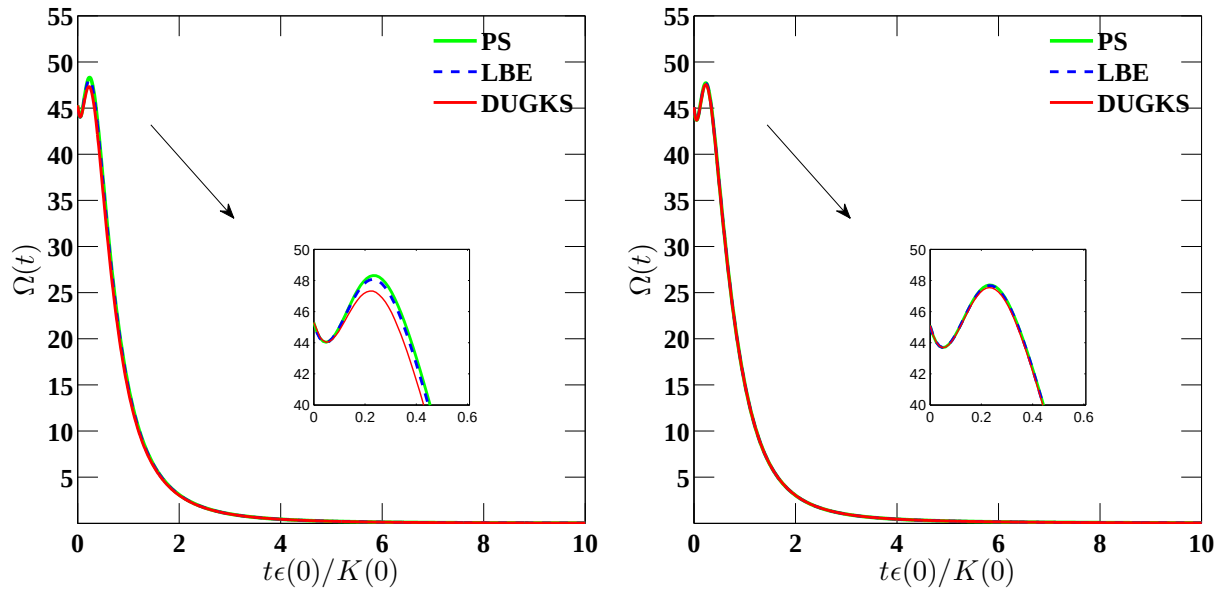

(a) (b)

FIG. 8: Evolutions of the enstrophy Ω with different mesh resolutions of (a) $N^3 = 128^3$ and (b) $N^3 = 256^3$ at $\mathrm{Re}_\lambda = 26.06$.

tion rate $\epsilon(t)/\epsilon_0$. As shown in Fig. 7, both $K(t)/K_0$ and $\epsilon(t)/\epsilon_0$ calculated by LBE and DUGKS methods are in excellent agreement with those from PS simulation on both meshes. Quantitatively, we compare the the maximum errors of $K(t)$ and $\epsilon(t)$ relative to the PS results, which is defined by

$$R_m(s) = \left\| \frac{s - s_p}{s_p} \right\|_{max}, \tag{37}$$

where $s = K(t)$ or $\epsilon(t)$, and s_p is the corresponding quantity from the PS method. Here we assume that the flow is regarded as adequately resolved when the relative error of the dissipation rate $R(\epsilon)$ is less than 4%. As shown in Table II, the maximum relative errors are less than 1% except that of $\epsilon(t)$ from the DUGKS with $N^3 = 128^3$ which reaches to 3.9% around the peak value, and it decreases to 0.49% in the 256^3 simulation. Although these discrepancy can be seen more clearly from the evolution of the enstrophy shown in Fig. 8a, the maximum relative difference is less than 4%, which means that the given flow is adequately resolved by the DUGKS with the minimum spatial resolution parameter $k_{max}\eta = 3.12$. Moreover, these difference can be reduced by using the finer mesh with the minimum $k_{max}\eta = 6.24$ as shown in Fig. 8b, which indicates that the DUGKS is more dissipative than the LBE method. We also observe that the normalized energy dissipation rate attains a peak value at $t' = 0.23$ due to the energy cascade, before decreasing with increasing time due to the viscous dissipation.

TABLE II: The maximum errors of $K(t)/K_0$ and $\epsilon(t)/\epsilon_0$ relative to PS results.

Case	LBE128	LBE256	DUGKS128	DUGKS256
$R_m(K)$	0.42%	0.34%	0.84%	0.49%
$R_m(\epsilon)$	0.83%	0.31%	3.90%	0.49%

Thirdly, we compare the evolutions of the Kolmogorov length λ and the Taylor microscale length η. The Kolmogorov length is the smallest scale in turbulence flow, at which the viscous effect dominates and the turbulence kinetic energy is converted irreversibly into heat. The Taylor micro-scale is the intermediate scale between the largest and the smallest scales at which fluid viscosity significantly affects the dynamics of turbulent eddies in the flow. Figures 9 and 10 show the evolutions of the Kolmogorov length scale and Taylor micro-scale length. It is found that results of both scales from the DUGKS and the LBE methods agree well with those from the PS method. We also note that there are slightly differences around

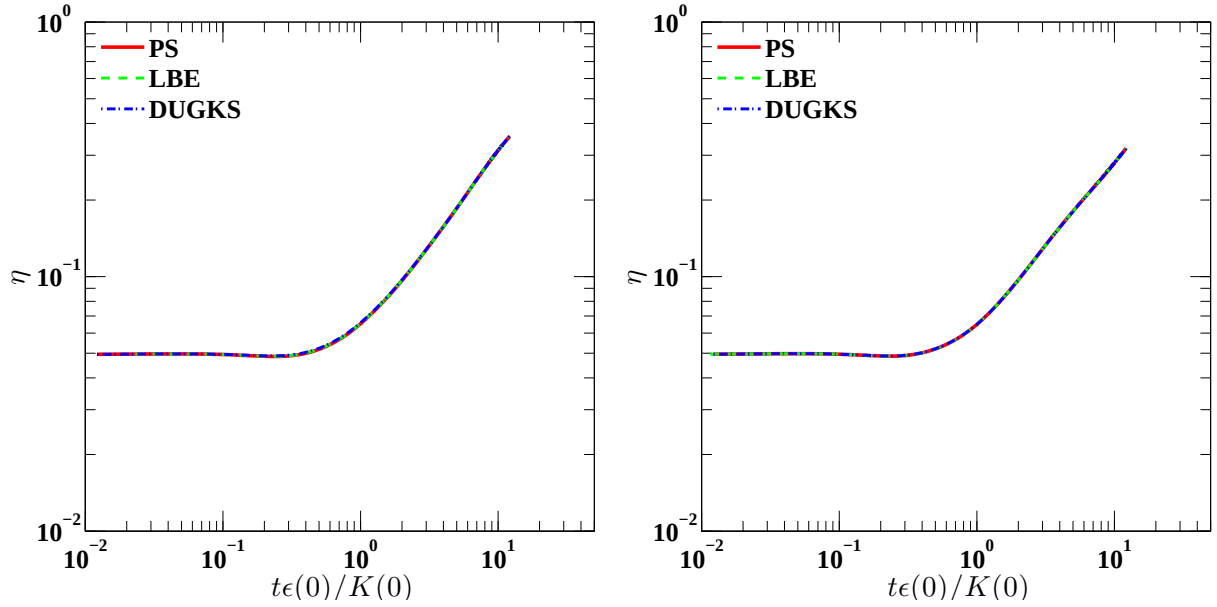

FIG. 9: Evolutions of the Kolmogorov length η with different mesh resolutions of (a) $N^3 = 128^3$ and (b) $N^3 = 256^3$ at $\mathrm{Re}_\lambda = 26.06$.

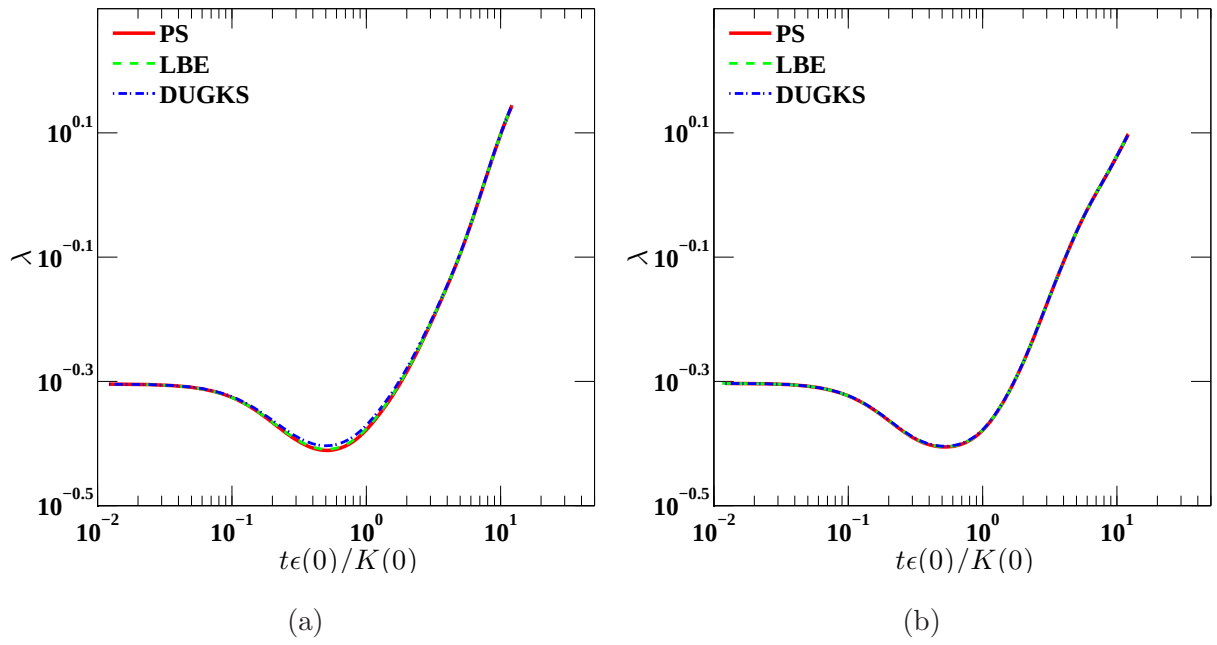

FIG. 10: Evolutions of the Taylor microscale length λ with different mesh resolutions of (a) $N^3 = 128^3$ and (b) $N^3 = 256^3$ at $\mathrm{Re}_\lambda = 26.06$.

the minimum of λ obtained by the DUGKS with the mesh resolution of 128^3, but as shown in Table III, the maximum relative errors of λ and η are all less than 2%, and reduce to 0.27% as the resolution increases to 256^3.

TABLE III: The maximum errors of λ and η relative to PS results.

Case	LBE128	LBE256	DUGKS128	DUGKS256
$R_m(\lambda)$	0.21%	0.08%	1.00%	0.12%
$R_m(\eta)$	0.44%	0.12%	1.84%	0.27%

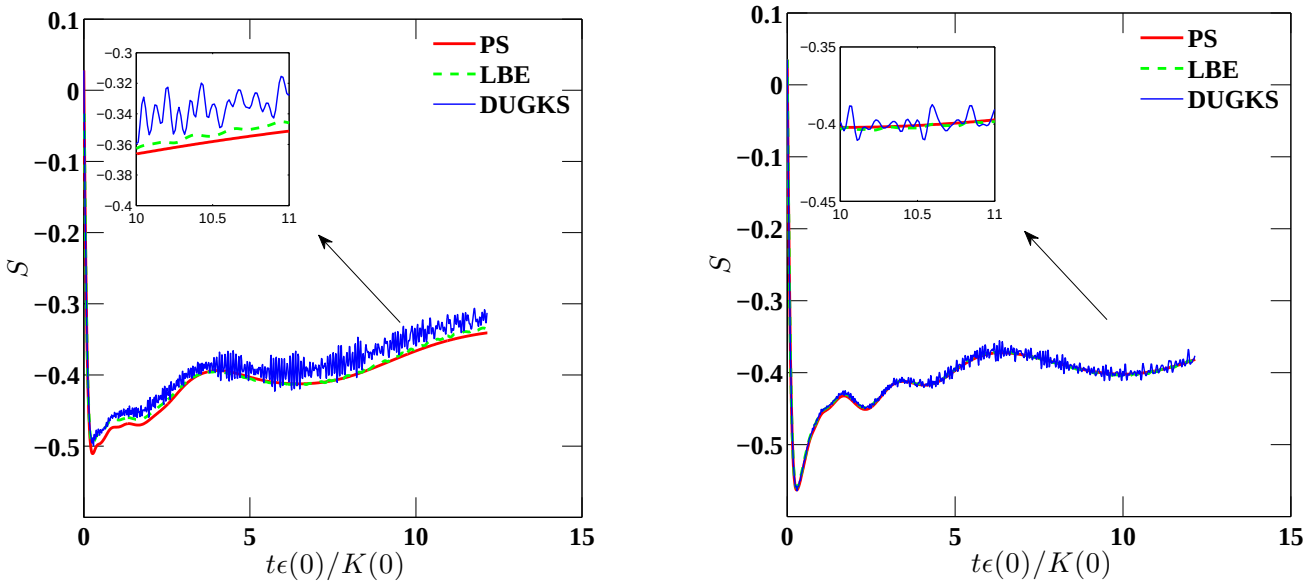

FIG. 11: Evolutions of velocity-derivative skewness S with different mesh resolutions of (a) $N^3 = 128^3$ and (b) $N^3 = 256^3$ at $\mathrm{Re}_\lambda = 26.06$.

The time evolutions of the averaged velocity-derivative skewness and flatness predicted by these three methods are shown in Figs. 11 and 12, respectively. It can be seen that the results of LBE with the mesh of 128^3 are in good agreement with the PS solutions, while those of the DUGKS show some high frequency oscillations, although the tendency agrees reasonably with the results from the PS simulation. The oscillations can be attributed to the acoustic waves in the system. The remarkable discrepancy between the LBE and DUGKS results may be caused by the following reasons: firstly, in the MRT-LBE model, the bulk viscosity can

be adjusted by tuning the relaxation time s_1 to absorb the acoustic waves, whereas the BGK based DUGKS doesn't have such a dissipation mechanism due to the single relaxation time in the BGK equation. Actually, the results of MRT-LBE with small bulk viscosity also have high frequency oscillations shown in Ref. [17], where the bulk viscosity $\zeta = 0.0273$ compared to $\zeta = 0.1134$ in the present simulation; secondly, since the velocity-derivative skewness and flatness are the third order and four order moments of $\nabla \boldsymbol{u}$, respectively, it is a significant challenge for a second-order method to compute such high-order quantities that are governed by small scales. As demonstrated, both the LBE and DUGKS methods have small numerical dissipation so that both methods can accurately compute the low-order statistic quantities that are governed by large scales. But the numerical dissipation of DUGKS is slightly larger than the LBE method, and yet, the absent acoustic-wave dissipation mechanism enlarges the discrepancy as the velocity field decays and consequently results in errors in high-order quantities. The high-order errors, however, seem to have little impact on the kinetic energy and dissipation rate.

As previous noted, increasing the mesh resolution can reduce the numerical dissipation, thus better results should be obtained in 256^3 simulations. As expected, as shown in Figs. 11b

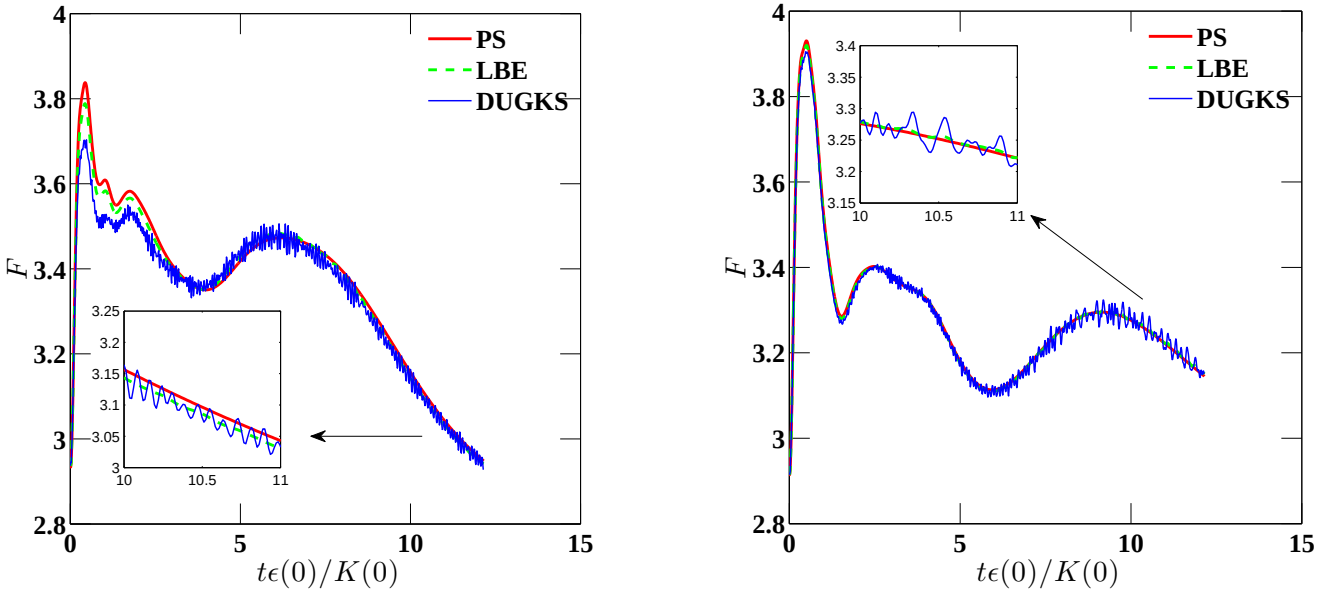

FIG. 12: Evolutions of velocity-derivative flatness F with different mesh resolutions of (a) $N^3 = 128^3$ and (b) $N^3 = 256^3$ at $\mathrm{Re}_\lambda = 26.06$.

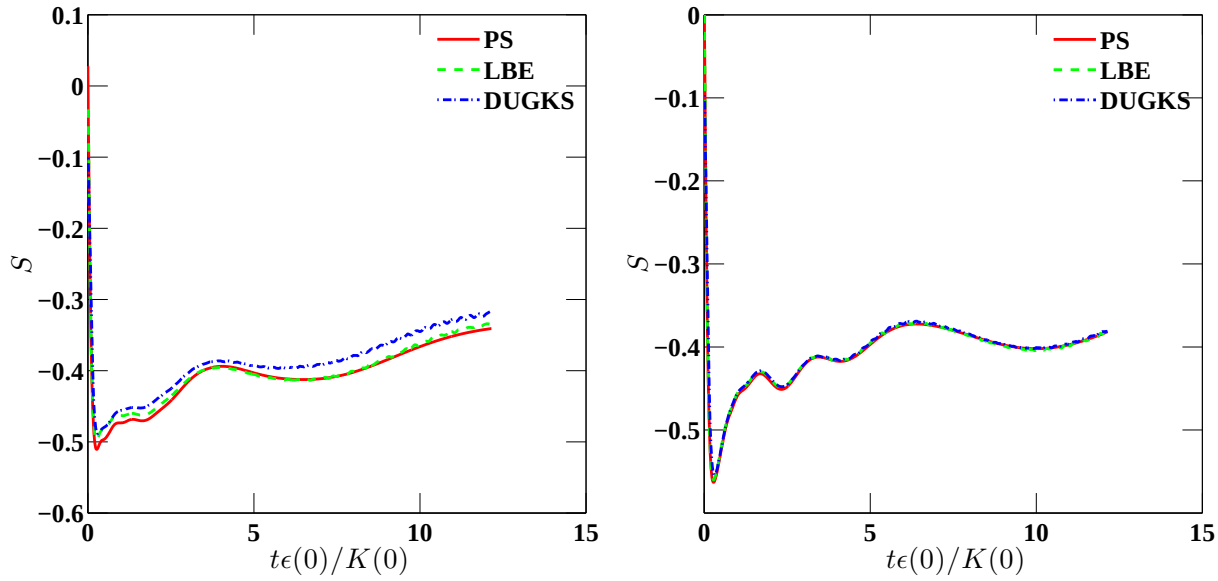

FIG. 13: Evolutions of smoothed velocity-derivative skewness S with different mesh resolutions of (a) $N^3 = 128^3$ and (b) $N^3 = 256^3$ at $\mathrm{Re}_\lambda = 26.06$.

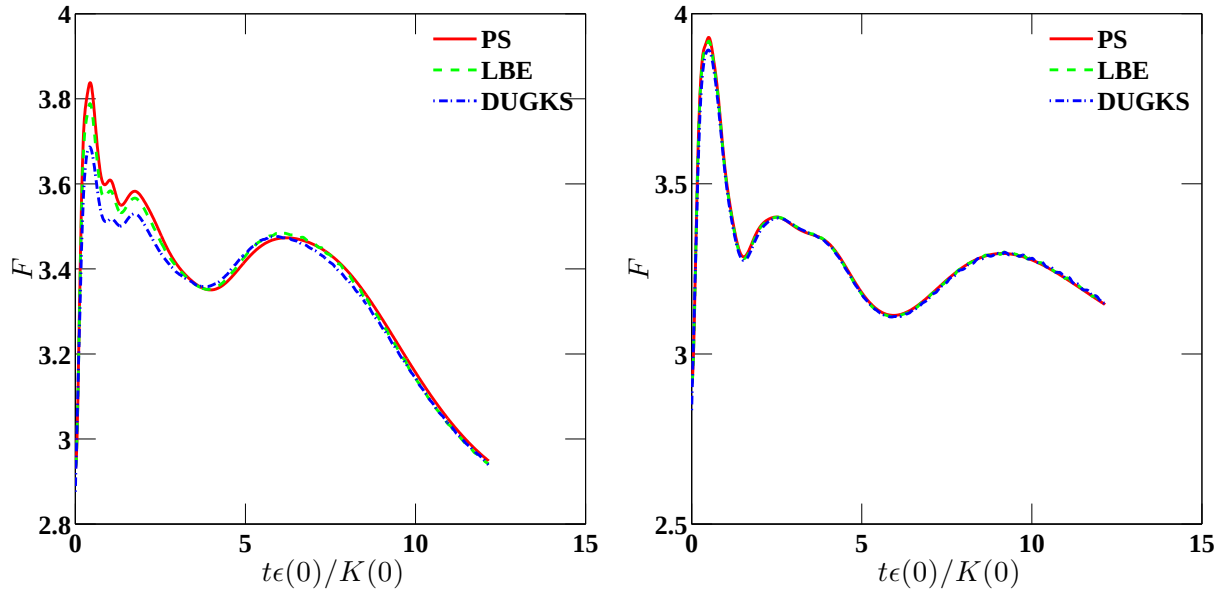

FIG. 14: Evolutions of smoothed velocity-derivative flatness F with different mesh resolutions of (a) $N^3 = 128^3$ and (b) $N^3 = 256^3$ at $\mathrm{Re}_\lambda = 26.06$.

and 12b, the results of DUGKS with $N^3 = 256^3$ are better than those with the coarse mesh, and the magnitudes of the oscillations are also reduced.

TABLE IV: The maximum errors of S and F relative to PS results.

Case	LBE128	LBE256	DUGKS128	DUGKS256
$R_m(S)$	3.35%	4.52%	11.97%	4.98%
$R_m(F)$	1.30%	0.35%	3.97%	1.11%

For convenient comparison, the results of the DUGKS can be filtered out by simple smoothing through averaging (using the smooth function in the matlab), as suggested in Ref. [17]. The smoothed skewness and flatness results are shown in Figs. 13 and 14, respectively. It is found that both LBE and DUGKS results indeed agree well with the PS results. Quantitatively, as given in Table IV, the maximum relative error of S predicted by the DUGKS with the mesh of 128^3 is 11.97%, while for the LBE, this value is 3.35%. As the resolution increases to 256^3, the maximum relative error of S computed by the DUGKS reduces to 4.98%.

4. Effects of the Reynolds number

In the above subsections, we have made some detailed comparisons between the LBE and DUGKS methods with the initial $\mathrm{Re}_\lambda = 26.06$, at which the initial flow fields can be well-resolved by both methods. In order to further compare the performance of the LBE and DUGKS methods at higher Re_λ, we conduct the DNS of the DHIT at $\mathrm{Re}_\lambda = 52.12$ and 104.24 with a fixed mesh of 128^3. Accordingly, in the PS simulation, the minimum spatial resolution parameters $k_{max}\eta$ are 1.33 for $\mathrm{Re}_\lambda = 52.12$ and 0.83 for $\mathrm{Re}_\lambda = 104.24$, suggesting that the PS method can adequately resolve the flow field at $\mathrm{Re}_\lambda = 52.12$ [50]. In addition, values of the minimum $k_{max}\eta$ for LBE and DUGKS with mesh of 128^3 are 2 for $\mathrm{Re}_\lambda = 52.12$ and 1.26 for $\mathrm{Re}_\lambda = 104.24$, respectively, indicating that the flow at $\mathrm{Re}_\lambda = 52.12$ can be adequately resolved by the LBE method [17]. However, it is not clear whether this resolution is sufficient for the DUGKS method at these Re_λ. Herein we compare some key statistic quantities obtained by both kinetic approaches at these Re_λ with those from the PS simulations.

Figures 15 and 16 show the energy spectra $E(k,t)$ and the dissipation rate spectra $D(k,t)$

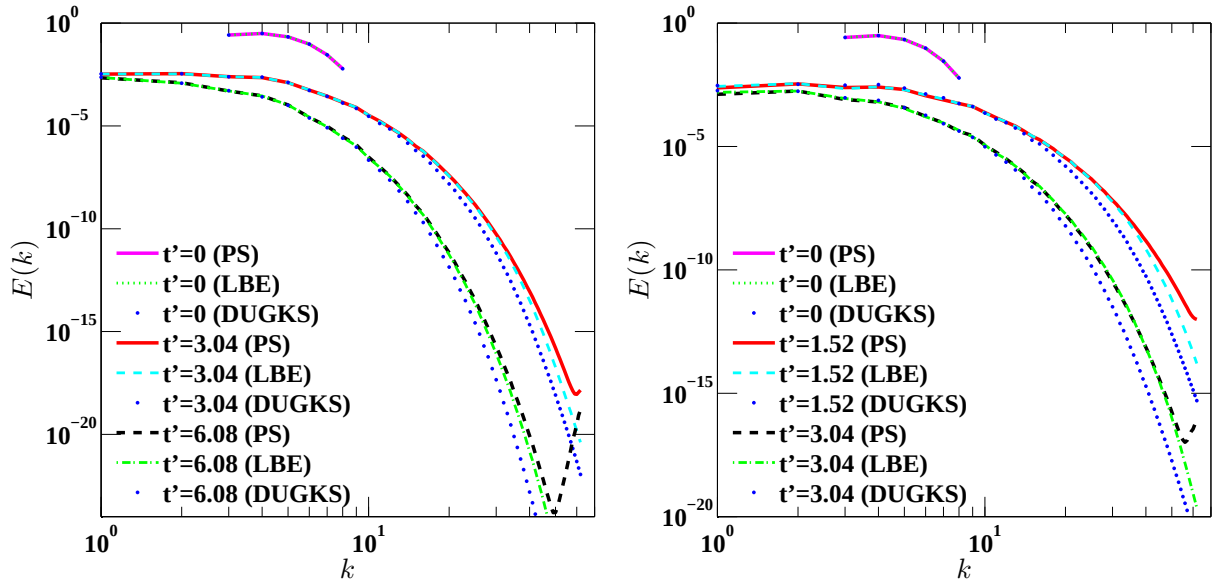

FIG. 15: The energy spectra $E(k,t)$ at (a) $\mathrm{Re}_\lambda = 52.12$ and (b) $\mathrm{Re}_\lambda = 104.24$.

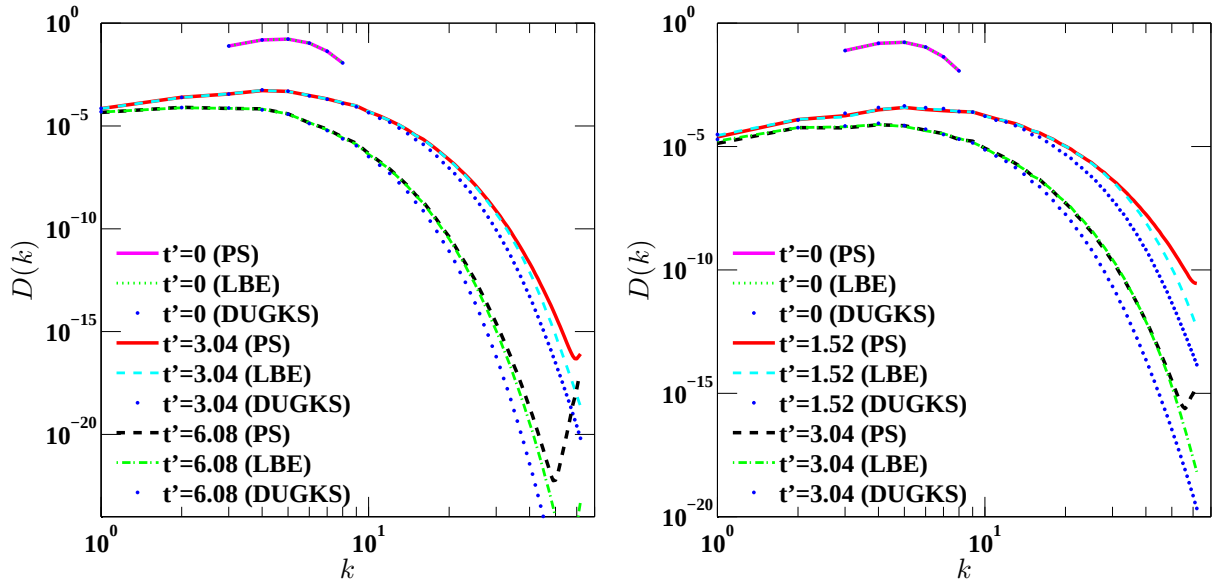

FIG. 16: The dissipation rate spectra $D(k,t)$ at (a) $\mathrm{Re}_\lambda = 52.12$ and (b) $\mathrm{Re}_\lambda = 104.24$.

at different times. It is observed that, $E(k,t)$ and $D(k,t)$ obtained by the LBE method are still in good agreement with those from the PS method, while the results from the DUGKS clearly deviate from the PS results in the high wavenumber region and the discrepancies increase with Re_λ. The differences of the spectra between both kinetic methods and the PS

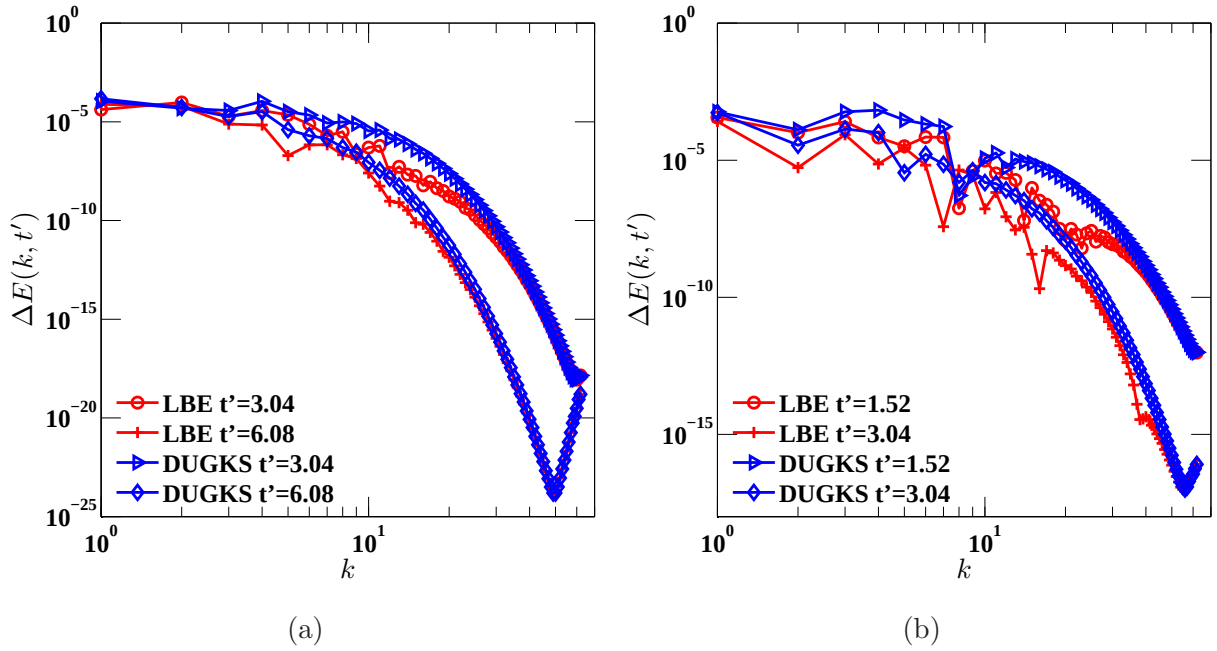

FIG. 17: The energy spectra difference $\Delta E(k,t')$ at (a) $\mathrm{Re}_\lambda = 52.12$ and (b) $\mathrm{Re}_\lambda = 104.24$.

method, as defined by Eq. (36), are shown in Figs. 17 and 18. It can be clearly seen that the LBE method yields better predictions than the DUGKS.

We also compare the evolutions of the normalized kinetic energy and the dissipation rate. As shown in Fig. 19, $K(t)/K_0$ obtained by LBE and DUGKS methods are in good agreements with the PS results. However, the differences are visible around the peak values of $\epsilon(t)/\epsilon_0$ computed by both methods, and it can be clearly seen that the LBE method gives a better prediction than the DUGKS. For example, at $\mathrm{Re}_\lambda = 52.12$, for the LBE the maximum relative error of ϵ is 1.85%, while for the DUGKS that is 11.6%. This indicates that with the minimum $k_{max}\eta = 2.0$ the given flow field is well resolved by the LBE method, but not the DUGKS. Similar phenomena can also be observed from the evolution of the enstrophy shown in Fig. 20 for the given Reynolds numbers, especially the discrepancy around the peak values as shown in the insets. The similar results are also obtained from the evolutions of the Kolmogorov length η and the Taylor micro-scale length λ, which are shown in Figs. 21 and 22, respectively. We observe that the maximum deviation appears around the minimums of η or λ, where the adequate spatial resolution in DUGKS and LBE is most likely not met. It can be clearly found that the LBE is more accurate than the DUGKS in capturing both scales due to the lower numerical dissipation in LBE.

Finally, in order to figure out the effects of Reynolds number on the flow fields for the

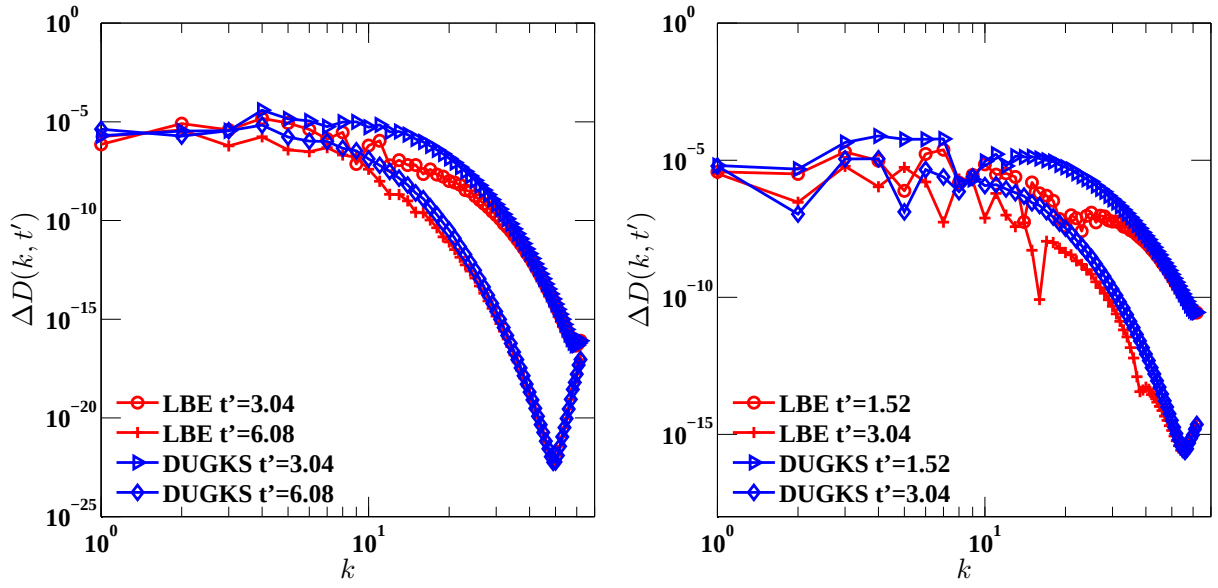

FIG. 18: The dissipation rate spectra difference $\Delta D(k,t)$ at (a) $\mathrm{Re}_\lambda = 52.12$ and (b) $\mathrm{Re}_\lambda = 104.24$.

DUGKS, we also compare the vorticity fields predicted by the both methods. Figs. 23 and 24 show the snapshots of the vorticity at $\mathrm{Re}_\lambda = 52.12$ and $\mathrm{Re}_\lambda = 104.24$, respectively. It can be clearly seen that the DUGKS results deviate from the LBE results at later times, and the difference is larger for larger Re. It should be noted that although in DUGKS the pressure fluctuation will increase with the Reynolds number under the given mesh resolution, these fluctuations do not deteriorate the flow fields, which are still smooth at high Re_λ as shown in Figs. 23 and 24.

Based on the above observations, we can conclude that the LBE gives more accurate results than the DUGKS at both Re_λ with under-resolved meshes. Specifically with the minimum spatial resolution parameter $2 < k_{max}\eta < 3$, the flow fields can be adequately resolved by the LBE method, but are not adequately resolved by the DUGKS, particularly in the high wave-number region which represents the small-scales turbulent eddies. This means that the DUGKS has relatively larger numerical dissipation than the LBE.

It is interesting to figure out the reasoning behind the more dissipative nature of the DUGKS than the LBE. One of the major reason is that as a finite volume scheme, additional numerical dissipation is introduced in the DUGKS in the the initial data reconstruction. It should be noted that although the DUGKS is more dissipative than the LBE method, we

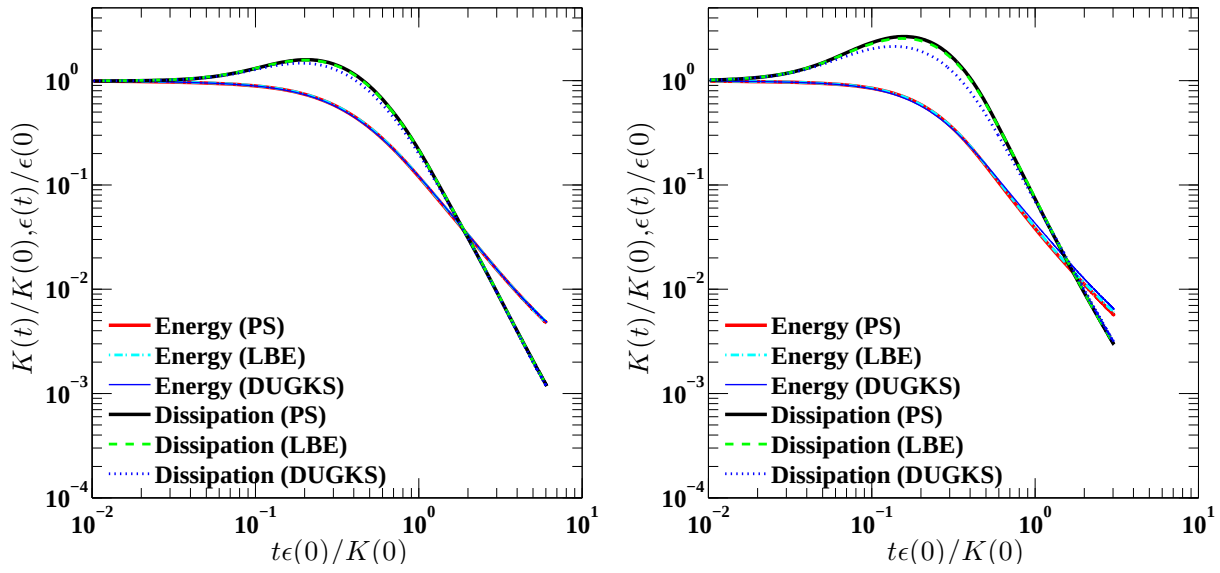

FIG. 19: Evolutions of the normalized total kinetic energy $K(t)/K_0$ and the normalized dissipation rate $\epsilon(t)/\epsilon_0$ at (a) $\mathrm{Re}_\lambda = 52.12$ and (b) $\mathrm{Re}_\lambda = 104.24$.

argue that the coupled collision and transport mechanism in the flux reconstruction can ensure that the DUGKS still has relatively low numerical dissipation when compared with the direct unwinding reconstruction of the original distribution function without considering the collision effects [43, 44]. It should be noted that the CFL number γ in DUGKS we adopt is 0.7071, which is relatively large for such kinetic scheme. Actually, since the physical model, rather than interpolation, is directly applied to reconstructed the flux across the cell interface, the dissipation will decrease with reducing CFL number or increasing the non-uniformities of the mesh according to the local accuracy requirement, which has been demonstrated in the previous work [45, 52].

5. *Computational efficiency and numerical stability*

Finally, we compare the computational efficiency of the LBE and DUGKS methods on a fixed mesh of 128^3. For each iteration, the CPU time costs of the LBE and DUGKS are 0.666s and 0.911s, respectively, where both codes run on 16 cores based on the message passing interface (MPI) using two dimensional domain decomposition. Therefore, the LBE method is about 36.8% faster than the DUGKS per time step. But, owing to the different time-steps used in the two methods, in our simulations two DUGKS time steps are equivalent

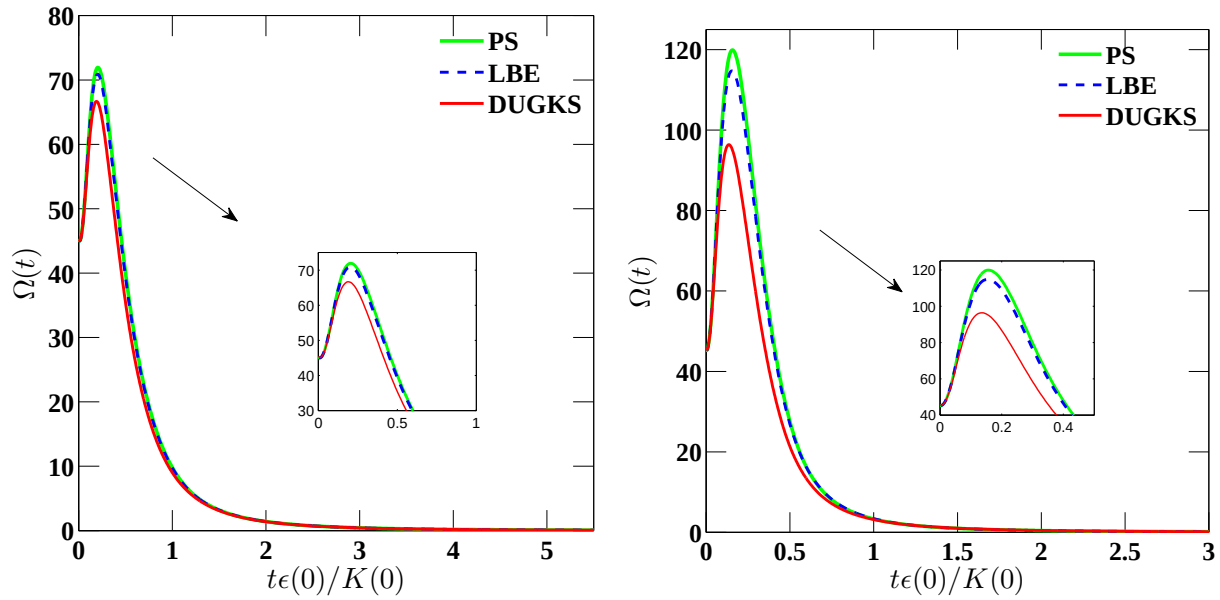

FIG. 20: Evolutions of the enstrophy Ω at (a) $\mathrm{Re}_\lambda = 52.12$ and (b) $\mathrm{Re}_\lambda = 104.24$.

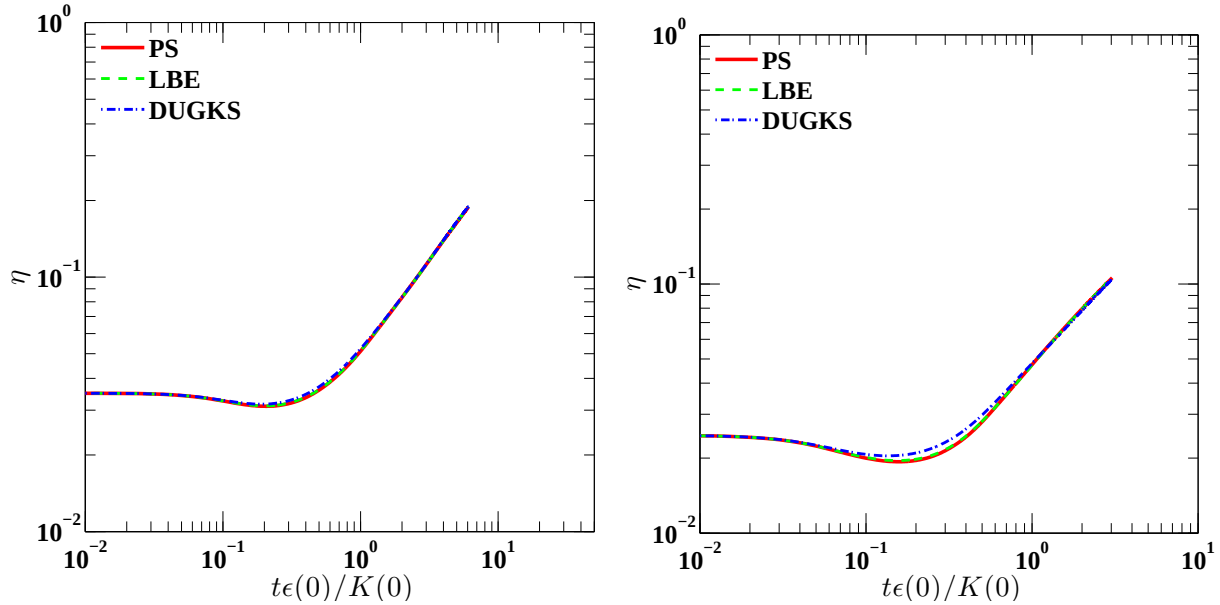

FIG. 21: Evolutions of the Kolmogorov length η at (a) $\mathrm{Re}_\lambda = 52.12$ and (b) $\mathrm{Re}_\lambda = 104.24$.

to one LBE time step .

In terms of the numerical stability, we compute the maximum stable Taylor microscale Reynolds number of both LBE and DUGKS codes on a mesh of 128^3. In the simulations,

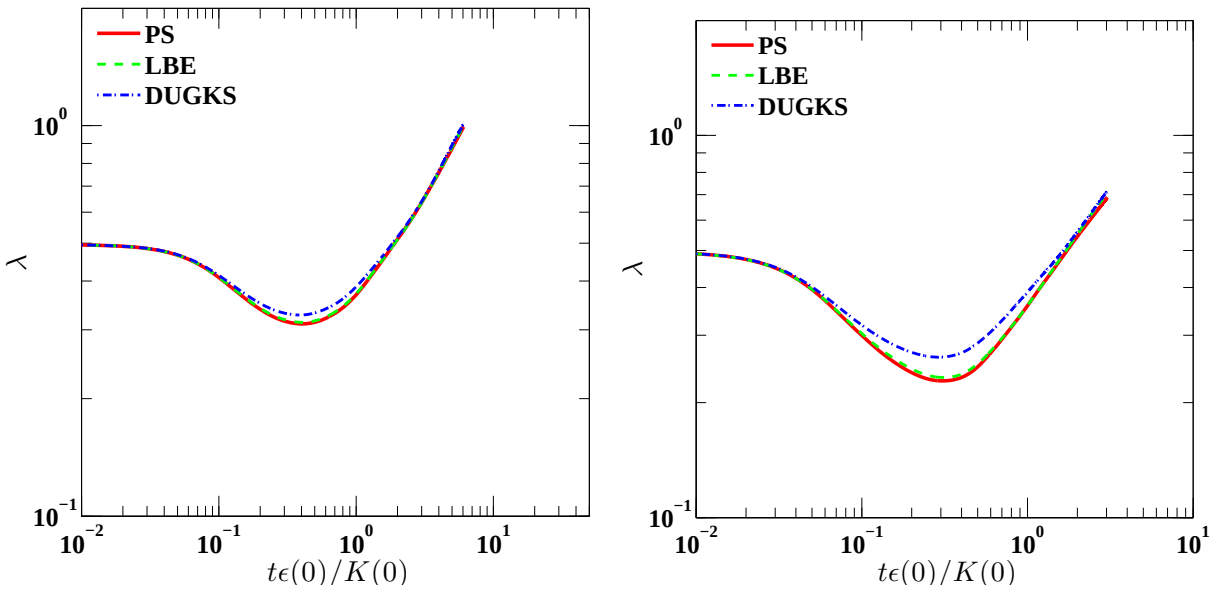

FIG. 22: Evolutions of the Taylor microscale length λ at (a) $\mathrm{Re}_\lambda = 52.12$ and (b) $\mathrm{Re}_\lambda = 104.24$.

we set the CFL number to be 0.9 in the DUGKS in order to make a fair comparison with the LBE in which the CFL number equals 1.0. Without considering the accuracy, the LBE code blows up when the Taylor microscale Reynolds number reaches $\mathrm{Re}_\lambda = 26060$, while the DUGKS is still stable at such Re_λ. Therefore, the DUGKS is more stable than the LBE methods, which is consistent with the previous study [45].

B. Kida vortex flow

The above results indicate that the flow can be adequately resolved by the DUGKS with the minimum spatial resolution parameter $k_{max}\eta$ larger than 3. In order to further validate this conclusion as well as the accuracy of the DUGKS for DNS of decaying turbulent, in this subsection the Kida vortex flow is simulated by the DUGKS, and compared with the well resolved LBE results.

1. Initial condition

The Reynolds number for the Kida vortex flow is defined by $\mathrm{Re} = LU_0/\nu$, where L is the domain size and ν is the kinematic viscosity. The initial pressure field as well as a consistent

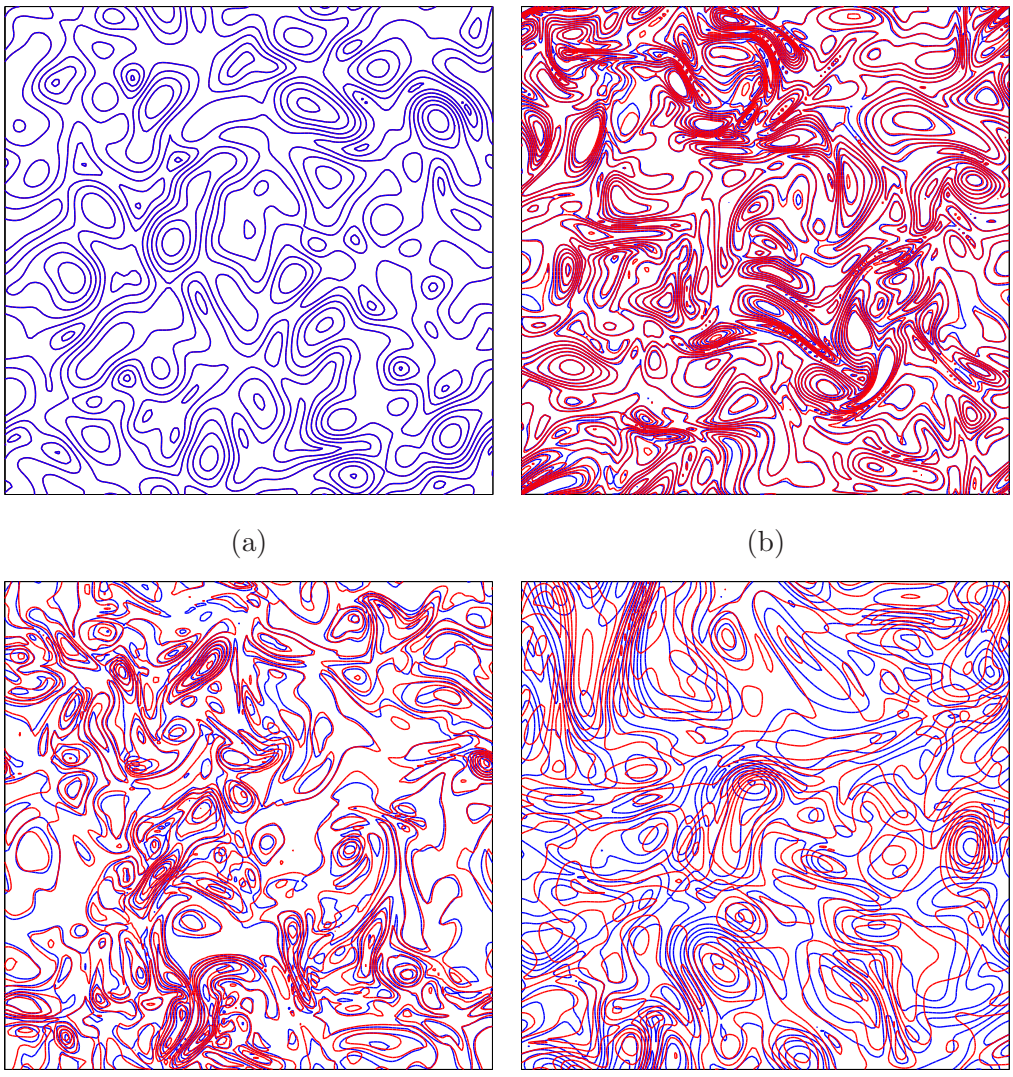

FIG. 23: Contours of normalized vorticity magnitude $\|\boldsymbol{\omega}\|L/u_0'$ on the xy plane at $z = L/2$ at time (a) $t' = 0$, (b) $t' = 0.12$, (c) $t' = 0.6$ and (d) $t' = 3$ for $\mathrm{Re}_\lambda = 52.12$. The solid red and blue lines denote results of the LBE and DUGKS, respectively.

initial distribution are obtained by an iterative procedure with the given initial velocity field (Eq. 32) [51].

In the simulation, we set the domain size $L = N$, where N is the grid size in each direction. The velocity and time presented in the results are normalized by U_0 and L/U_0, respectively. It should be noted that the previous results have clearly demonstrated that the accuracy of the standard LBE method is comparable to the PS method and the LBE can give the well-resolved result when the minimum spatial resolution parameter $k_{max}\eta$ is larger than 2.0 [17], thus for the Kida vortex flow simulation, the LBE results are adopted

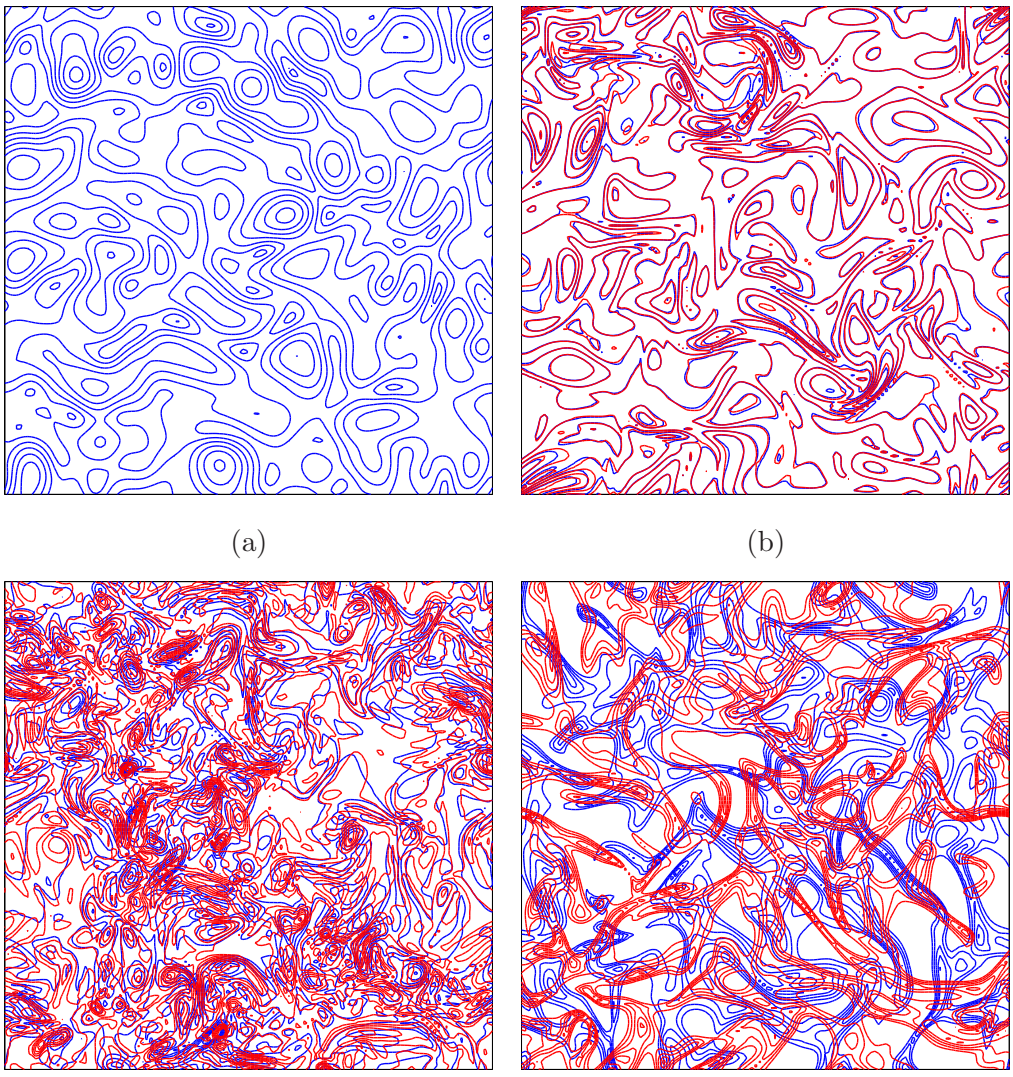

FIG. 24: Contours of normalized vorticity magnitude $\|\boldsymbol{\omega}\|L/u_0'$ on the xy plane at $z = L/2$ at time (a) $t' = 0$, (b) $t' = 0.1$, (c) $t' = 0.5$ and (d) $t' = 1.5$ for $\mathrm{Re}_\lambda = 104.24$. The solid red and blue lines denote results of the LBE and DUGKS, respectively.

as benchmark data to validate the accuracy of the DUGKS.

The simulation is performed for a relative low Reynolds number Re = 2000, which is sufficient for comparison. We set the computational domain size $L^3 = 256^3$ with mesh of $N^3 = 256^3$, and the corresponding minimum $k_{max}\eta$ is 3.29, which guarantees that the results obtained by LBE are adequately resolved. The velocity U_0 is set to be 0.05 such that the flow is nearly incompressible, and the CFL number is again set to be $\gamma = 0.7071$ so that the time step Δt in DUGKS is equal to 0.5.

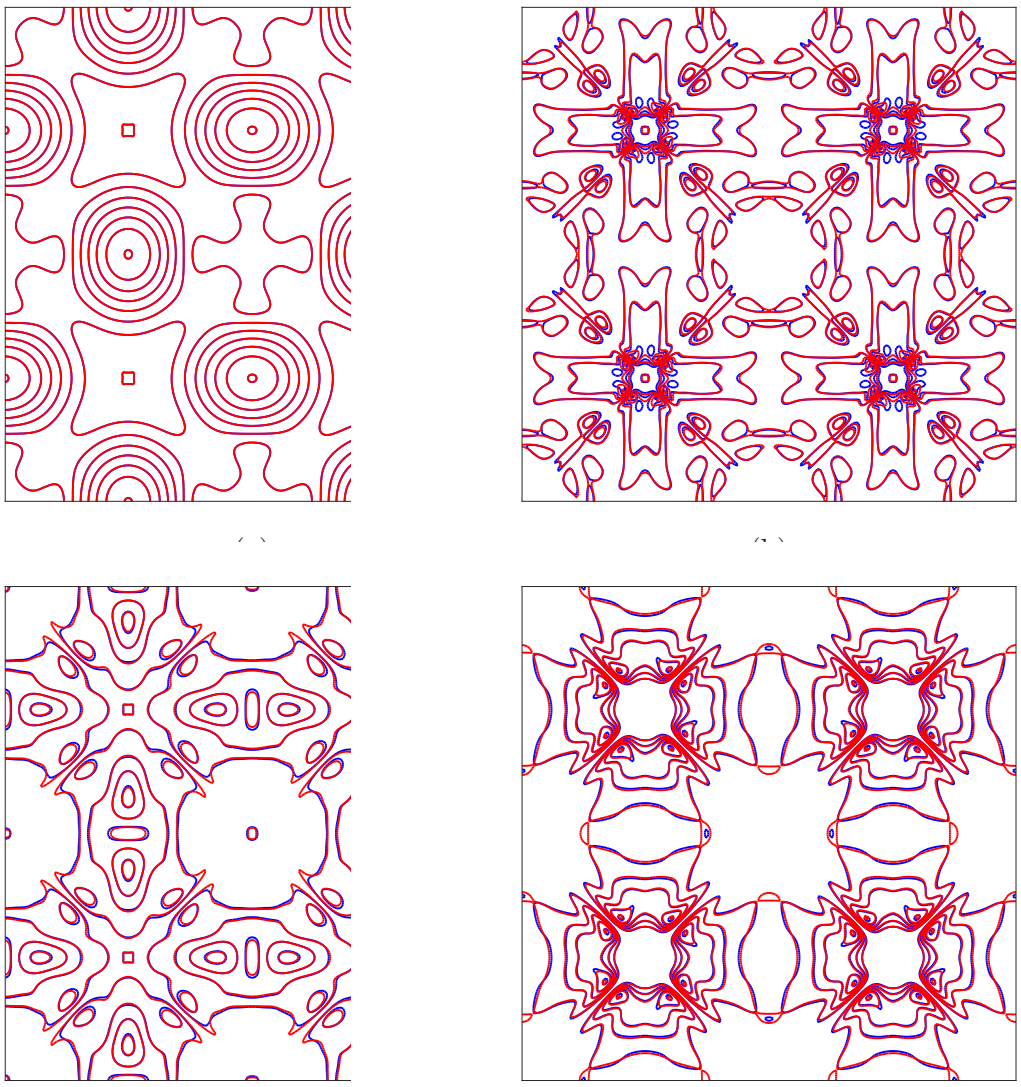

(c) (d)

FIG. 25: Contours of the normalized vorticity magnitude $\|\boldsymbol{\omega}\|L/u_0'$ on the xy plane at $z = L/2$ at time (a) $t' = 0$, (b) $t' = 0.9765$, (c) $t' = 1.9531$ and (d) $t' = 2.9297$ for $\mathrm{Re} = 2000$ with the mesh of 256^3. The solid blue and red lines denote results of the LBE and DUGKS, respectively.

2. Instantaneous vorticity fields

Figure. 25 shows the normalized vorticity $\|\omega\|L/U_0$ on the xy plane of $z = L/2$ at different normalized times $t = 0, 0.9765, 1.9531$ and 2.9297. As shown in Fig. 25a, both the LBE and DUGKS methods have identical initial fields containing only large eddies. These large eddies are unstable, and produce small eddies by vortex stretching as shown in Figs. 25b and 25c. In the end, as shown in Fig. 25d, the small eddies are dissipated by the viscous actions. In

addition, it is found that although vorticity snapshots predicted by the LBE and DUGKS methods are very similar to each other in terms of the vortex shapes and locations at the initial stage, the discrepancy between the two methods is still visible and increases over time. All these results are similar with those of the DNS of DHIT.

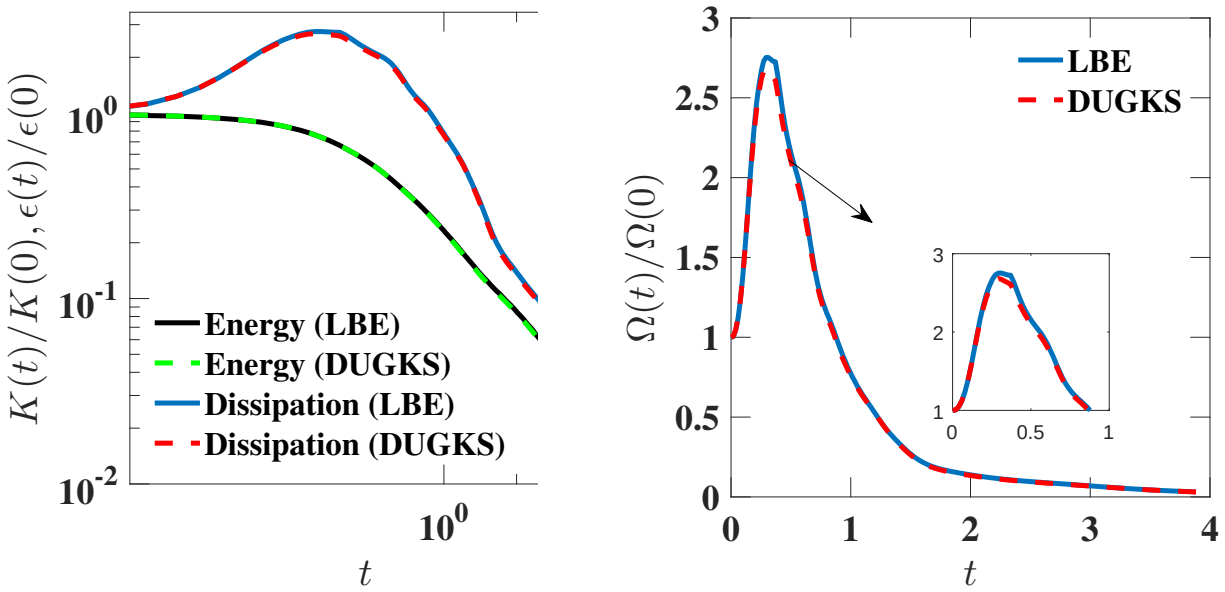

FIG. 26: Evolutions of (a) the normalized total kinetic energy K, dissipation rate ϵ and (b) enstrophy Ω.

3. *Statistical quantities*

We firstly study of the one point statistics of the Kida vortex flow. Fig. 26a shows the evolution of the normalized kinetic energy K and dissipation rate ϵ obtained from the LBE and DUGKS methods. As shown, the results of K and ϵ calculated by the DUGKS agree well with the LBE results. Particularly, the maximum relative error of dissipation rate compared to LBE results is less than 4%, which shows that the flow is adequately resolved by DUGKS with the minimum spatial resolution parameter $k_{max}\eta = 3.29$. Similar results are also obtained from the evolution of the enstrophy as shown in Fig. 26b, where the maximum relative error of the enstrophy is also less than 4%.

In order to further measure the capability of DUGKS in capturing the small scale, the evolution of Kolmogorov length scale is sketched in Fig. 27a, and the results obtained by LBE with the mesh of 256^3 are also included for comparison. As shown, the turbulent scale,

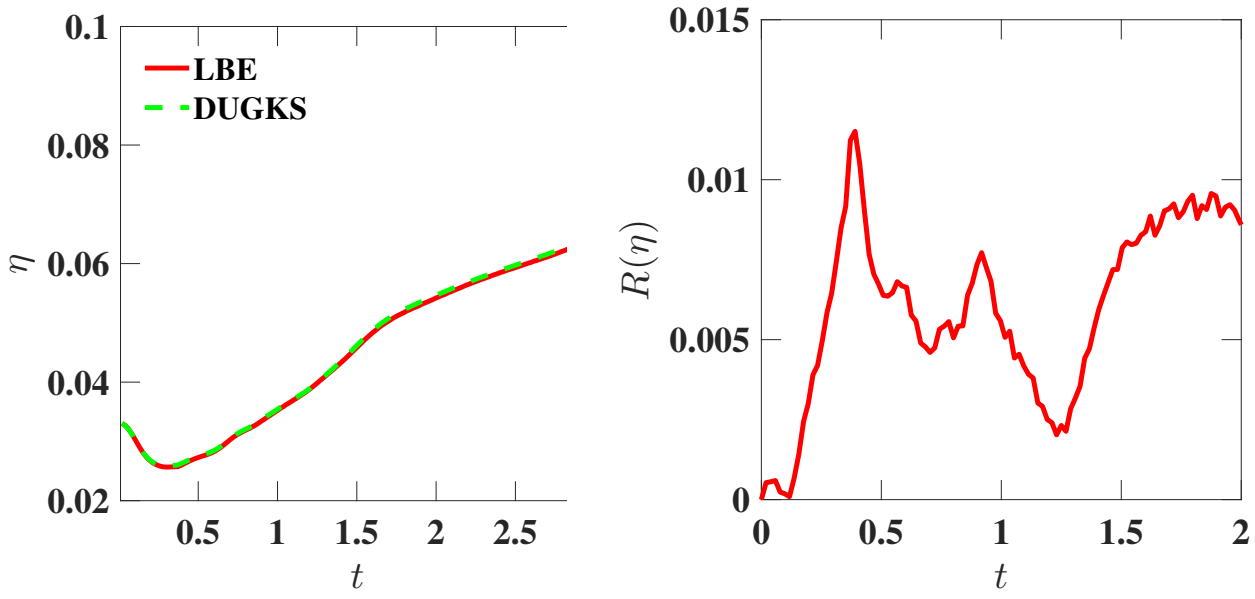

(a) (b)

FIG. 27: Evolutions of (a) Kolmogorov length scale η and (b) the relative difference $R(\eta)$ between the results of DUGKS and LBE on the mesh of 128^3.

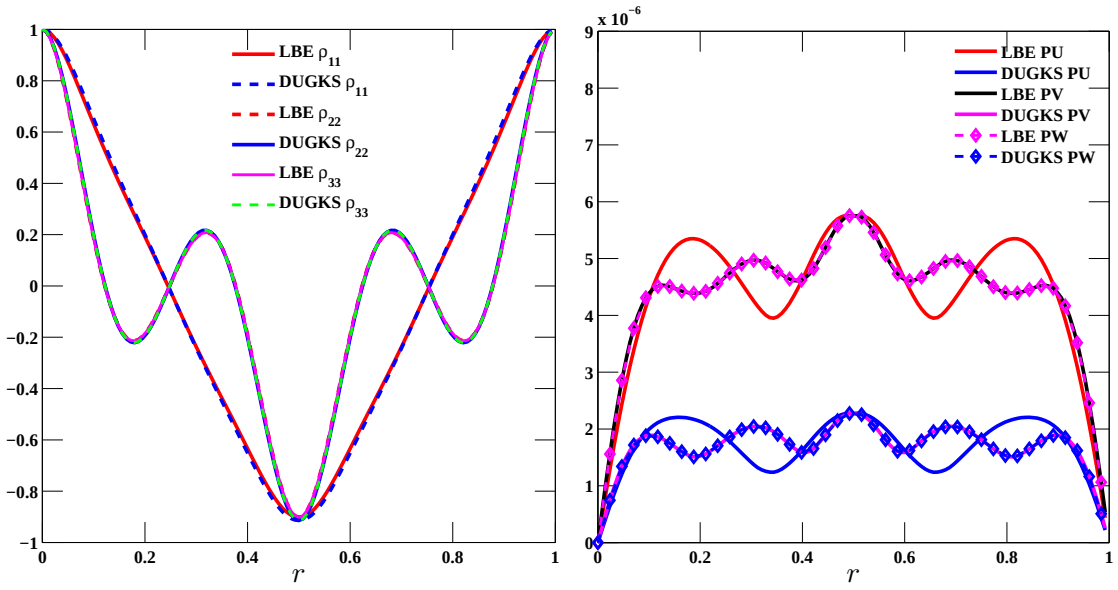

(a) (b)

FIG. 28: Comparisons of (a) the two-point longitudinal correlation(ρ_{11}), transversal correlations(ρ_{22}, ρ_{33}), and (b) the pressure-velocity correlations (PU, PV and PW) at $t = 1.95$.

from the large scale in the beginning to the smallest scale at about $t = 0.3$, can be described accurately, and the maximum relative error to LBE results, as shown in Fig. 27b, is less than 1.5%. It indicates that the flow is adequately resolved by the DUGKS with the minimum $k_{max}\eta = 3.29$. It is also found from Fig. 27a that owning to the viscous action, the small eddies are dissipated, and the scale of the eddies becomes larger as time evolves.

Figure. 28a shows the longitudinal and transverse correlation functions obtained from the LBE and DUGKS methods at $t = 1.95$. It can be seen that for both correlation functions, the LBE and DUGKS results agree well with each other, and the two transverse correlation functions, ρ_{22} and ρ_{33}, are identical due to the isotropic property of the Kida vortex flow.

Figure. 28b shows the pressure-velocity correlations predicted by the LBE and DUGKS methods at $t = 1.95$. Since the Kida vortex flow considered here is incompressible, thus, theoretically the pressure-velocity correlations defined by Eq. (35) are equal to 0 . As shown in Fig. 28b, although the values predicted by DUGKS are larger than those from the LBE method, the magnitude of the pressure velocity correlations given by both methods are on the order of 10^{-6}, which indicates that the DUGKS can accurately reproduce the incompressibility behavior.

V. DISCUSSIONS AND CONCLUSIONS

In this work, we present a comparative study of two kinetic approaches, the LBE and DUGKS methods, for direct numerical simulation of the decaying turbulent flows, including the decaying homogeneous isotropic turbulence (DHIT) and the Kida vortex flow. Although the DNS of DHIT and Kida vortex flow are easily achievable, it is the first and essential step to validate the DUGKS method before it is used to simulate more complex turbulent flows.

In our study, we first perform the DNS of DHIT using LBE, DUGKS and PS methods at two mesh resolutions (128^3 and 256^3) at $\mathrm{Re}_\lambda = 26.06$, where the minimum spatial resolution parameters $k_{max}\eta$ are about 3.12 for the LBE and DUGKS methods and 2.07 for the PS method. In terms of accuracy, we first compare the instantaneous flow fields. It is found that the instantaneous velocity and vorticity fields predicted by both LBE and DUGKS methods are very similar to each other and agree reasonably well with the PS results. In addition, we compare some key statistic quantities, and find that both methods perform an accurate prediction on all the quantities of interest due to their low numerical dissipation. We also note that the DUGKS with a coarse mesh of 128^3 underestimates the energy and dissipation

rate spectra in the high wavenumber region, and yet, these discrepancies vanish with the fine mesh of 256^3. This indicates that the DUGKS has a relatively large numerical dissipation compared with the LBE method, which can be attributed to the finite volume formulation of the DUGKS and the central difference employed in DUGKS to approximate the gradient at the cell interface. Furthermore, since the numerical viscosity ($0.5{c_s}^2\Delta t$) in LBE method has been explicitly subtracted, so it is not surprising that the LBE method has relatively small numerical dissipation. However, as the numerical results shown, this feature has little impact on the low order statistic quantities, and the flow can be adequately resolved by the DUGKS method with the minimum $k_{max}\eta > 3$. Moreover, we observe that the results of skewness and flatness obtained by the DUGKS have high frequency oscillations due to the acoustic waves in the system.

The performance of the two methods at higher Reynolds numbers are also compared. Some key statistic quantities obtained by LBE and DUGKS methods are compared with those from the PS method. The results show that good agreements are achieved between the LBE and the PS methods at both Re_λ, but there are noticeable discrepancies between the results of DUGKS and PS methods due to the insufficient mesh resolution, which also indicates that the DUGKS is more dissipative than the LBE method.

In order to further evaluate the accuracy of the DUGKS, the direct numerical simulation of the Kida vortex flow is also performed with a relatively low Reynolds number, and the results are validated by those from LBE method. The simulations are conducted with the minimum $k_{max}\eta = 3.29$, which guarantees that the results from the LBE method are adequately resolved. The results show that although DUGKS is slightly more dissipative than the LBE method, it can accurately predict the low order statistics, such as the total energy and its dissipation rate, enstrophy, the longitudinal and transversal velocity correlations, and capture the smallest Kolmogorov length scale in turbulent flow. The results of the pressure-velocity correlation also show that the DUGKS can well reproduce the incompressibility behavior of the flow.

In terms of the computational efficiency, the LBE method is about 36.8% faster than the DUGKS per time step. It should be noted that although the DUGKS is less efficient than the LBE method on the same uniform mesh, as a finite volume method, the DUGKS can use non-uniform meshes without additional efforts for wall-bounded turbulence flows, such as a channel flow and pipe flow. For such flows, the mesh can be clustered near the walls where large flow gradients exist, and the computational efficiency can be largely improved,

which will be presented in our subsequent work. We also assess the numerical stability of the LBE and DUGKS methods by computing the maximum stable Taylor micro-scale Reynolds number on a fixed mesh without considering the accuracy. The results show that the DUGKS has a better numerical stability than the LBE method, which is consistent with the previous results of laminar flows [45].

In conclusion, the LBE is less dissipative and thus more accurate than the DUGKS, but they have similar accuracy for DNS of the decaying turbulent flows when the mesh resolution is sufficient to resolve the flow field; in addition, the DUGKS is less efficient than the LBE method with the same regular uniform mesh, but superior to the LBE method in terms of the numerical stability; furthermore, it is found that the DUGKS can adequately resolve the flow when the minimum spatial resolution parameter $k_{max}\eta$ is about 3, which is a more strict requirement when compared to $k_{max}\eta > 2$ for LBE [17] and $k_{max}\eta > 1$ for the pseudo-spectral method [50]. It must be emphasized that this work is the first step to validate the DUGKS for DNS of turbulent flows, and further tests are needed before regarding it as a viable kinetic method for DNS of turbulent flows. The main advantage of the DUGKS compared with the LBE method is that it can be implemented on non-uniform meshes easily, which we shall demonstrate in the subsequent study of wall-bounded turbulent flows.

ACKNOWLEDGMENT

The authors acknowledge the support by the National Natural Science Foundation of China (Grant No. 51125024) and the U.S. National Science Foundation (NSF) under grants CNS1513031, CBET-1235974, and AGS-1139743.

---

[1] S. B. Pope, *Turbulent flows* (Cambridge University Press, 2000).

[2] H. Le, P. Moin, and J. Kim, Journal of Fluid Mechanics **330**, 349 (1997).

[3] P. Moin and K. Mahesh, Annual Review of Fluid Mechanics **30**, 539 (1998).

[4] R. D. Moser, J. Kim, and N. N. Mansour, Physics of Fluids **11**, 943 (1999).

[5] B. Van Leer, AIAA paper **2520**, 2001 (2001).

[6] H. Xu, W. Tao, and Y. Zhang, Physics Letters A **373**, 1368 (2009).

[7] H. Chen, S. Kandasamy, S. Orszag, R. Shock, S. Succi, and V. Yakhot, Science **301**, 633 (2003).

[8] H. Chen, S. Chen, and W. H. Matthaeus, Physical Review A **45**, R5339 (1992).

[9] D. O. Martinez, W. H. Matthaeus, S. Chen, and D. Montgomery, Physics of Fluids **6**, 1285 (1994).

[10] S. Hou, J. Sterling, S. Chen, and G. Doolen, Pattern Formation and Lattice Gas Automata **6**, 149 (1996).

[11] J. G. Eggels, International Journal of Heat and Fluid flow **17**, 307 (1996).

[12] G. Amati, S. Succi, and R. Piva, International Journal of Modern Physics C **8**, 869 (1997).

[13] D. d'Humières, Philosophical Transactions of the Royal Society of London. Series A: Mathematical, Physical and Engineering Sciences **360**, 437 (2002).

[14] H. Yu, S. S. Girimaji, and L.-S. Luo, Journal of Computational Physics **209**, 599 (2005).

[15] H. Yu, S. S. Girimaji, and L.-S. Luo, Physical Review E **71**, 016708 (2005).

[16] H. Yu, L.-S. Luo, and S. S. Girimaji, Computers & Fluids **35**, 957 (2006).

[17] Y. Peng, W. Liao, L.-S. Luo, and L.-P. Wang, Computers & Fluids **39**, 568 (2010).

[18] H. Gao, H. Li, and L.-P. Wang, Computers & Mathematics with Applications **65**, 194 (2013).

[19] L.-P. Wang, C. Peng, Z. Guo, and Z. Yu, Computers & Fluids **124**, 226 (2016).

[20] S. Chikatamarla, C. Frouzakis, I. Karlin, A. Tomboulides, and K. Boulouchos, Journal of Fluid Mechanics **656**, 298 (2010).

[21] F. Bösch, S. S. Chikatamarla, and I. V. Karlin, Physical Review E **92**, 043309 (2015).

[22] B. Dorschner, F. Bösch, S. Chikatamarla, K. Boulouchos, and I. Karlin, Journal of Fluid Mechanics **801**, 623 (2016).

[23] W. Liao, Y. Peng, and L.-S. Luo, AIAA Paper **548**, 2008 (2008).

[24] W. Liao, Y. Peng, and L.-S. Luo, Physical Review E **80**, 046702 (2009).

[25] W. Liao and L. Luo, AIAA Paper **586**, 2009 (2009).

[26] G. Kumar, S. S. Girimaji, and J. Kerimo, Journal of Computational Physics **234**, 499 (2013).

[27] M. Righi and R. Wang, in *Proceedings of the 29th International Symposium on Rarefied Gas Dynamics*, Vol. 1628 (AIP Publishing, 2014) pp. 1363–1370.

[28] S. Chen and G. D. Doolen, Annual Review of Fluid Mechanics **30**, 329 (1998).

[29] S. Succi, *The Lattice-Boltzmann Equation* (Oxford University Press, Oxford, 2001).

[30] C. K. Aidun and J. R. Clausen, Annual Review of Fluid Mechanics **42**, 439 (2010).

[31] Z. Guo and C. Shu, *Lattice Boltzmann method and its applications in engineering (advances in computational fluid dynamics)* (World Scientific Publishing Company, 2013).

[32] L.-S. Luo, M. Krafczyk, and W. Shyy, Encyclopedia of Aerospace Engineering (2010).

[33] Z. Guo, K. Xu, and R. Wang, Physical Review E **88**, 033305 (2013).

[34] Z. Guo, R. Wang, and K. Xu, Physical Review E **91**, 033313 (2015).

[35] L. Zhu, Z. Guo, and K. Xu, Computers & Fluids **127**, 211 (2016).

[36] N. Cao, S. Chen, S. Jin, and D. Martinez, Physical Review E **55**, R21 (1997).

[37] Z. Guo and T.-S. Zhao, Physical Review E **67**, 066709 (2003).

[38] G. Peng, H. Xi, C. Duncan, and S.-H. Chou, Physical Review E **59**, 4675 (1999).

[39] N. Rossi, S. Ubertini, G. Bella, and S. Succi, International Journal for Numerical Methods in Fluids **49**, 619 (2005).

[40] S. Ubertini and S. Succi, Progress in Computational Fluid Dynamics, an International Journal **5**, 85 (2005).

[41] S. Ubertini and S. Succi, Communications in Computational Physics **3**, 342 (2008).

[42] T. Lee and C.-L. Lin, Journal of Computational Physics **171**, 336 (2001).

[43] T. Ohwada, Journal of Computational Physics **177**, 156 (2002).

[44] S. Chen and K. Xu, Journal of Computational Physics **288**, 52 (2015).

[45] P. Wang, L. Zhu, Z. Guo, and K. Xu, Communications in Computational Physics **17**, 657 (2015).

[46] P. L. Bhatnagar, E. P. Gross, and M. Krook, Physical Review **94**, 511 (1954).

[47] X. He and L.-S. Luo, Journal of Statistical Physics **88**, 927 (1997).

[48] B. Keating, G. Vahala, J. Yepez, M. Soe, and L. Vahala, Physical Review E **75**, 036712 (2007).

[49] L. Biferale, P. Gualtieri, and F. Toschi, Physics of Fluids (1994-present) **12**, 1836 (2000).

[50] V. Eswaran and S. Pope, Computers & Fluids **16**, 257 (1988).

[51] R. Mei, L.-S. Luo, P. Lallemand, and D. dHumières, Computers & Fluids **35**, 855 (2006).

[52] L. Zhu, P. Wang, and Z. Guo, arXiv preprint arXiv:1511.00242 (2015).